Out of the Dark and into the Light
Microscopic Analysis of Bright, Dark and Trapped Excitons

Maja Feierabend

Department of Physics

CHALMERS UNIVERSITY OF TECHNOLOGY

Göteborg, Sweden 2018

Out of the Dark and into the Light
Microscopic Analysis of Bright, Dark and Trapped Excitons

Maja Feierabend

Cover illustration: Activation of dark excitons via molecules.

Out of the Dark and into the Light
Microscopic Analysis of Bright, Dark and Trapped Excitons
Maja Feierabend
Department of Physics
Chalmers University of Technology

Abstract

Atomically thin transition metal dichalcogenides (TMDs) have been in the focus of current research due to their efficient light-matter interaction, as well as the remarkably strong Coulomb interaction that leads to tightly bound excitons. Due to their unique band structure, TMDs show a variety of optically accessible *bright* and inaccessible *dark* excitons. Moreover, due to their optimal surface-to-volume ratio, these materials are very sensitive to changes in their surroundings, which opens up the possibility of externally tailoring their optical properties.

The aim of this thesis is to present different strategies to control the optical fingerprint of TMD monolayers via molecules, strain and impurities. Based on a fully quantum-mechanical approach, we show that the coupling of excitons to high-dipole molecules can activate dark excitonic states, resulting in an additional and well-pronounced peak in the optical spectra.

Moreover, we find that these dark excitonic states are very sensitive to strain, leading to crucial energy shifts and intensity changes of the dark exciton signature. Our findings reveal the potential for optical sensing of strain through activation of dark excitons.

Finally, we investigate the possibility of local impurities to trap excitons resulting in *localized* states. We study the formation, excitonic binding energies and wave functions of localized excitonic states, all of which depend on the trapping potential. With this, we are able to calculate the photoluminescence signal and investigate the possibility of single-photon emission.

List of publications

I. **Dark excitons in transition metal dichalcogenides**
E. Malic, M. Selig, M. Feierabend, S. Brem, D. Christiansen, F. Wendler,
A. Knorr, G. Berghaeuser
Phys. Rev. Materials 2, 014002 (2018)

II. **Optical fingerprint of non-covalently functionalized transition
metal dichalcogenides**
M. Feierabend, E. Malic, A. Knorr, and G. Berghaeuser
J. Phys. Condens. Matter 29, 384003 (2017)

III. **Proposal for dark exciton based chemical sensors**
M. Feierabend, G. Berghaeuser, A. Knorr, and E. Malic
Nature Commun. 8, 14776 (2017)

IV. **Molecule signatures in photoluminescence spectra of transi-
tion metal dichalcogenides**
M. Feierabend, G. Berghaeuser, M. Selig, S. Brem, T. Shegai, S. Eigler,
E. Malic
Phys. Rev. Materials 2, 014004 (2018)

V. **Optical response from functionalized atomically thin nanoma-
terials**
E. Malic, G. Berghaeuser, M. Feierabend, and A. Knorr
Annalen der Physik 1700097 (2017)

VI. **Impact of strain on the optical fingerprint of monolayer tran-
sition metal dichalcogenides**
M. Feierabend, A. Morlet, G. Berghaeuser, E. Malic
Phys. Rev. B 96, 045425 (2017)

VII. **Impact of strain on the excitonic linewidth in transition metal
dichalcogenides**
Z. Khatibi, M. Feierabend, M. Selig, S. Brem, C. Linderaelv, P. Erhart,
and E. Malic
In review process (2018)

VIII. **Dark-exciton based strain sensing in transition metal dichalco-genides**
M. Feierabend, Z. Khatibi, G. Berghaeuser, E. Malic
In review process (2018)

My contributions to the appended papers

II.-IV, VI, VIII.: As first-author, I developed the theoretical model, performed the numerical evaluation, analyzed the results and wrote the papers with the help of my main supervisor.

VII: As second-author, I contributed by performing calculations, analyzing the results and writing parts of the paper.

I., V. : As co-author, I contributed by performing calculations and helped analyzing the results.

Contents

1 Introduction

A material consisting of atoms arranged in a hexagonal lattice and only one atom thick was long considered a purely theoretical construction. Hence the discovery of graphene, a single layer of carbon atoms, in 2004 by A. Geim and K. Novoselov was a breakthrough, which was rewarded with the Nobel Prize in physics in 2010 [1].

Besides its incredible properties in strength, heat and electrical conductance and transparency, graphene paved the way for a new class of materials, the so called 2D materials. Consisting of only a few layers of atoms, these materials show unique properties compared to their 3D counterparts which brought them into the focus of nowadays research and thousands of materials are just waiting to be discovered.
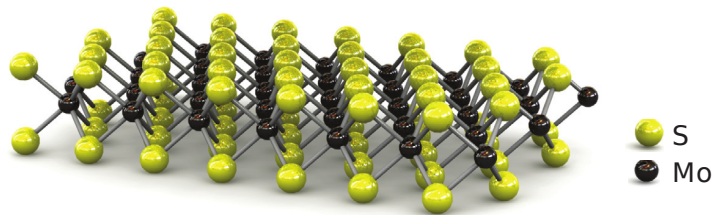

Figure 1: **Schematic view of a TMD monolayer.** The side view of a monolayer of transition metal dichalcogenides is shown, with black representing M=(Mo,W) atoms and yellow representing X=(S,Se) atoms. Both M and X layers exhibit a honeycomb-like structure, similar to graphene. Figure taken from [2].

Transition metal dichalcogenides (TMDs) are a promising example, in which a layer of transition metal (W, Mo, Te) is sandwiched between two layers of chalcogenides (S, Se). These materials exhibit, in contrast to graphene, a rich band structure with direct and indirect band gaps, and a strong optical response. Moreover, due to their low dimensionality, 2D materials exhibit interesting phenomena: (i) strongly bound electron-hole pairs, so called excitons, caused by Coulomb interaction [3–8] and (ii) sensitivity to their environment due to their optimal surface-to-volume ratio [9–13]. It has been shown that the optical response in TMDs is dominated by excitons [14–16],

and hence it is crucial to understand the formation, relaxation and interaction of excitons on a microscopic level.

Besides bright (optically accessible) excitons, TMDs also exhibit a variety of (i) dark (optically forbidden) excitons [4, 9, 17–27], which are either spin- or momentum forbidden, and (ii) localized excitons [28–30] due to trapping potentials. Hence the optical response of TMDs is crucially influenced by the landscape of excitons.
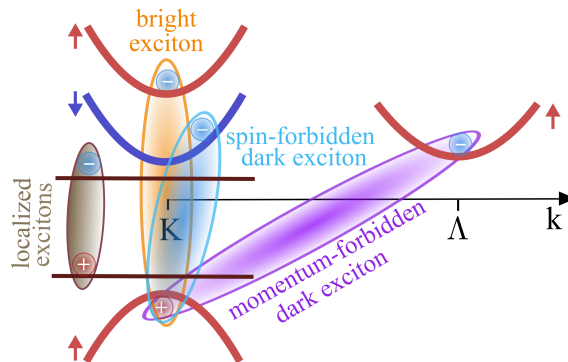

Figure 2: **The variety of excitons.** Electronic dispersion around the high symmetry K and Λ points in the Brillouin zone. Beside bright excitons (yellow), i.e. both electron and hole have the same spin and momentum, there also exist dark (not optically active) excitons. Dark states can be either spin (blue) or momentum (purple) forbidden. Besides, due to local changes in the band structure, states within the band gap can appear which give rise to the formation of localized excitons (brown) [31].

The aim of this thesis is to investigate the interplay of bright, dark and localized excitons in TMDs by developing a microscopic framework. Moreover, we show that due to the low dimensionality TMDs are extremely sensitive to their environment, such as attached molecules, strain and impurities. Within our framework we are able to calculate optical absorption and photoluminescence spectra and the changes associated with it.

The obtained insights shed light on processes on a microscopic level and might inspire future experiments towards technical applications, such as molecule and strain sensing through activation of dark states or single photon emission from localized states.

2 Theoretical Framework

The aim of this thesis is to understand the optical properties of TMDs on a microscopic level, in particular the response of the system after optical excitation. To reach this goal, we use the density matrix formalism to account for the many-particle interactions [5, 32, 33] within the framework of the second quantization. By exploiting the Heisenberg equation of motion, we get access to equations of motion for microscopic polarization and occupations which describe the dynamics of our system.

In the Hamilton operator we include free-particle interactions, Coulomb contributions, interaction with phonons and any interaction with external parameters, such as molecules, strain or disorder [4, 25, 34].

By exploiting the cluster expansion and tight-binding approach we finally find the TMD Bloch equations which describe the carrier dynamics of the TMD and give access to the optical response.

2.1 Absorption Coefficient

The absorption coefficient $\alpha(\omega)$ is proportional to the optical susceptibility $\chi(\omega)$ as the linear response to an optical perturbation induced by an external vector potential $A(\omega)$

$$\alpha(\omega) \propto \omega \Im\left[\chi(\omega)\right] \propto \Im\left[\frac{j(\omega)}{\omega A(\omega)}\right] \tag{2.1}$$

and can be calculated with the macroscopic current density $j(\omega)$. To get access to microscopic quantities, we can quantize the field and express the current density within the second quantization using the definition [32]

$$\mathbf{j}(t) = \frac{e}{2m_0} \sum_{\mathbf{l_1 l_2}} \langle \Psi_{\mathbf{l_1}} | \mathbf{p} - e\mathbf{A}(\mathbf{r},t) | \Psi_{\mathbf{l_2}} \rangle \langle a_{\mathbf{l_1}}^{\dagger} a_{\mathbf{l_2}} \rangle + c.c. \tag{2.2}$$

with elementary charge e, electron mass m_0 and momentum operator $\mathbf{p}$. Here, we have introduced the electron annihilation (creation) operators $a_{\mathbf{l}}^{(\dagger)}$ and wave functions $\Psi_{\mathbf{l}}$.

Within the dipole approximation , i.e. $\mathbf{A}(\mathbf{r},t) \approx \mathbf{A}(t)$, and introducing the

carrier-light matrix element $M_{\mathbf{ij}} = \langle \Psi_{\mathbf{i}} | \mathbf{p} | \Psi_{\mathbf{j}} \rangle$ we can rewrite Eq. (2.1) and find for the absorption coefficient

$$\alpha(\omega) \propto \Im \left[\frac{\sum_{\mathbf{l_1 l_2}} M^*_{\mathbf{l_1 l_2}} p_{\mathbf{l_1 l_2}}(\omega) + c.c.}{\omega A(\omega)} \right] \qquad (2.3)$$

with the Fourier transformed microscopic polarization $p_{\mathbf{l_1 l_2}}(\omega) = \langle a^\dagger_{\mathbf{i}} a_{\mathbf{j}} \rangle$. Here, the compound index $\mathbf{i}$ includes momentum k_i, band λ_i and spin σ_i. We now have access to the absorption spectra on a microscopic level via the temporal evolution of $p_{\mathbf{ij}}$ which is obtained by the Heisenberg equation of motion [32, 35] $i\hbar \dot{p}_{\mathbf{ij}}(t) = [p_{\mathbf{ij}}, H]$. Here, H is the many-particle Hamilton operator and will be discussed in the next section.

2.2 Hamilton Operator

The many-particle Hamiltonian operator $H = H_0 + H_{c-l} + H_{c-c} + H_{imp} + H_{c-phon}$ includes:
(i) the non-interacting carrier contribution

$$H_0 = \sum_{\mathbf{l}} \epsilon_{\mathbf{l}} a^\dagger_{\mathbf{l}} a_{\mathbf{l}} + \hbar \omega_q c^\dagger_q c_q \qquad (2.4)$$

with the electronic band structure $\epsilon_{\mathbf{l}}$ [36, 37], electron annihilation (creation) operator $a_i^{(\dagger)}$ with momentum k_i, band λ_i and spin σ_i and photon annihilation (creation) operator $c^{(\dagger)}$;
(ii) the carrier-light interaction

$$\begin{aligned} H_{c-l} &= \frac{i\hbar e_0}{m_0} \sum_{\mathbf{l_1 l_2}} \mathbf{M_{l_1 l_2}} \mathbf{A(t)} \mathbf{a^\dagger_{l_1}} \mathbf{a_{l_2}} & (2.5) \\ &= \frac{i\hbar e_0}{m_0} \sum_{l_1 l_2 \mu} \left(g^\mu_{l_1 l_2} a^\dagger_{l_1} a_{l_2} c_\mu - g^{\mu*}_{l_1 l_2} a^\dagger_{l_2} a_{l_1} c^\dagger_\mu \right) & (2.6) \end{aligned}$$

with the electron mass m_0, elementary charge e_0 and the optical matrix element $M_{\mathbf{l_1 l_2}}$. Note that the first line is in the coherent limit where we use $A(r,t) \approx A(t)$ (semi-classical approach) and is used to calculate absorption spectra. The second line includes carrier-photon interaction and therefore represents the full quantum mechanical expression for the interaction with

4

light. The full quantum mechanical expression is needed to calculate the photoluminescence spectra. For details on the optical matrix elements see [4] or the theory part in PAPER IV or PAPER VI .
(iii) the carrier-carrier interaction

$$H_{c-c} = \frac{1}{2} \sum_{\mathbf{l_1 l_2 l_3 l_4}} V_{\mathbf{l_3 l_4}}^{\mathbf{l_1 l_2}} a_{\mathbf{l_1}}^{\dagger} a_{\mathbf{l_2}}^{\dagger} a_{\mathbf{l_4}} a_{\mathbf{l_3}} \qquad (2.7)$$

with Coulomb matrix element $V_{\mathbf{l_3 l_4}}^{\mathbf{l_1 l_2}}$ treated within the Keldysh formalism [38], for details see [4, 39], (iv) the carrier impurity interaction

$$H_{imp} = \sum_{\mathbf{l_1 l_2}} D_{\mathbf{l_1 l_2}} a_{\mathbf{l_1}}^{\dagger} a_{\mathbf{l_2}} \qquad (2.8)$$

with impurity coupling element $D_{\mathbf{l_1 l_2}}$ where the exact form of the coupling element depends on the form of impurities, and can be due to molecules, trapping potentials or strain; and
(v) the carrier phonon interaction

$$H_{c-phon} = \sum_{\mathbf{l_1 l_2}} G_{\mathbf{l_1 l_2 q}}^{\alpha} a_{\mathbf{l_1}}^{\dagger} a_{\mathbf{l_2}} (b_{\mathbf{q}}^{\alpha} + b_{-\mathbf{q}}^{\alpha\dagger}) \qquad (2.9)$$

with electron-phonon couplig element $G_{\mathbf{l_1 l_2 q}}^{\alpha}$ and phonon annihilation (creation) operator $b_q^{\alpha(\dagger)}$ with phonon mode α. The coupling elements are calculated by exploiting the nearest-neighbor tight binding approach [5, 32, 40]. Note that we include the electron-phonon interaction only indirectly via dephasing processes, for a detailed study on linewidth and scattering processes in TMDs see [24, 34]. We now have all ingredients to find the equation of motions for our system. Before this, we briefly want to introduce the TMDs special structure and the used tight-binding approach.

2.3   Transition Metal Dichalcogenides (TMDs)

Transition metal dichalcogenides (TMDs) consist of a layer of transition metal atom (Mo, W) sandwiched between two layers of dichalgonides (S, Se, T). Even though they have some dimension in z-direction and are not truly one-layer thick, we will call them 2D materials. The investigated TMDs are all semiconductors with band gaps in the range of 1.0 - 2.0 eV [16, 41, 42].
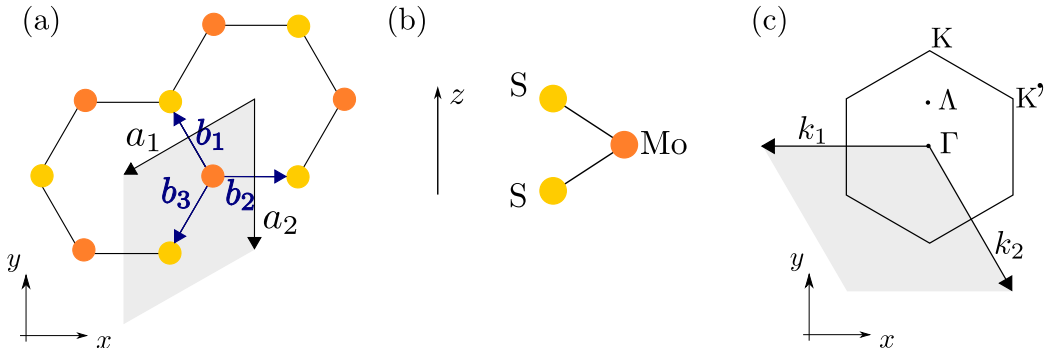
Figure 3: Schematic view to the MoS$_2$ layer. In (a) we see the honeycomb-like structure in real space in the xy plane with Molybdenum atoms in orange and sulfide atoms in yellow. Furthermore one can see the primitive cell in gray which is a rhombus as typically for hexagonal lattice structure and primitive vectors a_1 and a_2. Moreover we see the fundamental vectors b_j connecting Mo-and S-atoms. The structure is quasi 2D meaning that the height in z direction, cf. (b), is negligible small, here ≈ 0.3 nm. In (c) one can see the momentum space representation with reciprocal lattice and lattice vectors k_1 and k_2 and the high symmetry points K, K', Γ and Λ.

In comparison to graphene, TMD monolayer consists of two sub-lattices, cf. Fig. 3(a), one from the transition metal and one from the dichalcogenide. They both exhibit a hexagonal lattice and hence the S-lattice can be described simply by a translation of the Mo-lattice. The lattice in real space is described by primitive vectors $\mathbf{a}_1 = -\frac{a_0}{2} \begin{pmatrix} \sqrt{3} \\ 1 \end{pmatrix}$ and $\mathbf{a}_2 = -a_0 \begin{pmatrix} 0 \\ 1 \end{pmatrix}$. with lattice constant a_0.

For the primitive vectors in the momentum representation, cf. Fig. 3(c), one finds

$$\mathbf{k}_1 = -\frac{\pi}{a_0} \begin{pmatrix} \frac{4}{\sqrt{3}} \\ 0 \end{pmatrix}, \qquad \mathbf{k}_2 = \frac{\pi}{a_0} \begin{pmatrix} \frac{2}{\sqrt{3}} \\ 2 \end{pmatrix}. \tag{2.10}$$

Moreover, Fig.3(c) shows the most important symmetry points, namely K, K', Γ and Λ. Due to the two sub-lattices the inversion symmetry is broken and a direct band gap appears at the high symmetry K point. The electronic dispersion around the high symmetry points can be approximated by a parabolic band.

Electronic dispersion

To obtain the parabolic dispersion of the TMD structure one needs to solve Schrödingers equation

$$H\Psi_l = \epsilon_l \Psi_l \tag{2.11}$$

for the 2N particle system. We can make use of the tight-binding approach [4] which reads in the nearest-neighbor approximation:

$$\Psi_l(\mathbf{k},\mathbf{r}) = \frac{1}{\sqrt{N}} \sum_{j=\text{Mo,S}} C_j^l \sum_{\mathbf{R_j}} e^{i\mathbf{k}\cdot\mathbf{R}_j} \phi_j^l(\mathbf{r} - \mathbf{R}_j) \tag{2.12}$$

with N number of atoms, C_j^l the so called tight-binding coefficients, atomic orbitals $\phi_j^l(\mathbf{r} - \mathbf{R}_j)$ and vector $\mathbf{R}_j$ denoting the position of the atom within the sub-lattice j. Remember that we have a broken symmetry for K/K' points which means we have to solve Eq. (2.11) separately for both points, including also the two sub-lattices for Mo and S this leads us to four linear equations one has to solve. Close to the high-symmetry points one finds within a Taylor approximation for the electronic dispersion

$$\epsilon_\nu^l \approx \pm \left(\frac{\Delta E_\nu^{\lambda\sigma}}{2} + \frac{3|t^{\lambda\sigma}|^2}{4E_\nu^{\lambda\sigma}} \mathbf{k}^2 \right) \tag{2.13}$$

with valley index ν, bandgap energy $E_\nu^{\lambda\sigma} = E_{gap} + \nu E_{soc}^{\lambda\sigma}$ where E_{gap} is the bandgap energy and $E_{soc}^{\lambda\sigma}$ the spin depending band splitting. The $+$ corresponds to the K and $-$ to the K' point, respectively. The hopping integrals

$$t^{\lambda\sigma} = \langle \phi_j^{\lambda\sigma\nu}(\mathbf{r} - \mathbf{R}_j)|H|\phi_i^{\lambda\sigma\nu}(\mathbf{r} - \mathbf{R}_i)\rangle \tag{2.14}$$

which stem from the tight-binding approach determine the curvature of the corresponding band. The hopping integral will be important in Section 5.1 where we investigate the changes of this parameter due to strain. We can not solve those integrals within our theory but we can fix their values to the effective masses (taken from DFT/experiment [43]) s.t.

$$\frac{3|t^{\lambda\sigma}|^2}{4\Delta E_\nu^{\lambda\sigma}} = \frac{\hbar^2}{2m_{\text{eff}}}. \tag{2.15}$$

with effective mass m_{eff}.

2.4 TMD Bloch Equations

Once we have determined the full Hamiltonian we can now exploit Heisenberg's equation of motion $i\hbar\dot{x} = [x, H]$ where x are our microscopic quantities of interest. In particular, we are interested in:

1. Electron occupation $f_k^{\lambda\sigma} = \langle a_k^{\lambda\sigma\dagger} a_k^{\lambda\sigma} \rangle$

2. Polarization $p_{k_1 k_2}^{\lambda_1\sigma_1\lambda_2\sigma_2} = \langle a_{k_1}^{\lambda_1\sigma_1\dagger} a_{k_2}^{\lambda_2\sigma_2} \rangle$

3. Photon number $n_q^\mu = \langle c_q^{\mu\dagger} c_q^\mu \rangle$

4. Photo-Emission amplitude $S_{k_1 k_2 q}^{\lambda_1\sigma_1\lambda_2\sigma_2\mu} = \langle c_q^{\mu\dagger} a_{k_1}^{\lambda_1\sigma_1\dagger} a_{k_2}^{\lambda_2\sigma_2} \rangle$

5. Exciton occupation $F_{k_1 k_2 k_3 k_4}^{\lambda_1\sigma_1\lambda_2\sigma_2\lambda_3\sigma_3\lambda_4\sigma_4} = \langle a_{k_1}^{\lambda_1\sigma_1\dagger} a_{k_2}^{\lambda_2\sigma_2} a_{k_3}^{\lambda_3\sigma_3\dagger} a_{k_4}^{\lambda_4\sigma_4} \rangle$

Depending on the complexity of the system, we can look at different limits.

Coherent Limit

For the case of linear absorption spectra, we consider the driving field to be small and hence it is sufficient to take the coherent part of our quantities, i.e. we consider the photon density to be constant and the electron and exciton density changes to negligible small. Moreover, we treat the Coulomb interaction on the Hartree-Fock level which is an exact approximation in case of linear optics. With this, our key quantity is the microscopic polarization $p_{k_1 k_2}^{\lambda_1\sigma_1\lambda_2\sigma_2}$ which is a measure for optical transitions from states in the valence band with momentum k_1 to the conduction band with momentum k_2. Taking into account only spin allowed terms, i.e. $\sigma_1 = \sigma_2 = \uparrow$ we find for the

dynamical evolution

$$
i\hbar \frac{d}{dt} p_{\mathbf{k_1 k_2}}^{v\uparrow c\uparrow} = \left[\epsilon_{\mathbf{k_2}}^{c\uparrow} - \epsilon_{\mathbf{k_1}}^{v\uparrow} + \sum_{\mathbf{k'}} V_{\mathbf{k_1, k_2, k'}}^{ren} - i\gamma \right] p_{\mathbf{k_1 k_2}}^{v\uparrow c\uparrow} \tag{2.16}
$$

$$
- \sum_{\mathbf{k'}} V_{k', k_1, k_2}^{exc} p_{\mathbf{k_1 - k', k_2 - k'}}^{v\uparrow c\uparrow} \tag{2.17}
$$

$$
+ \frac{ie_0 \hbar}{m} \mathbf{M}_{\mathbf{k_1 k_2}}^{\mathbf{c\uparrow v\uparrow}} \cdot \mathbf{A(t)} \delta_{\mathbf{k_1 k_2}} \tag{2.18}
$$

$$
+ \sum_{\mathbf{k}} D_{k_2 k}^{cc} p_{k_1 k}^{v\uparrow c\uparrow} - D_{k k_1}^{vv} p_{k k_2}^{v\uparrow c\uparrow} \tag{2.19}
$$

where Eq. (2.16) is the electronic dispersion and Coulomb induced renormalization due to attractive electron-hole interaction, Eq. (2.17) the excitonic contribution stemming from the repulsive part of electron-hole interaction and leading to bound electron-hole pairs, Eq. (2.18) the light-matter interaction and Eq. (2.19) the interaction with via disorder. Interestingly, due to the disorder a momentum transfer between different polarization is possible. The dephasing γ includes both exciton-phonon interaction and radiative decay. This coupled set of equation is now solved numerically via a Runge Kutta method and finally gives us access to $p(t)$ which can be transformed by simple Fourier transformation to $p(\omega)$ and then by exploiting the Elliott formula, Eq. (2.3), we have access to the absorption spectra.

However, most experiments actually investigate the photoluminescence spectra of these materials. In order to theoretical calculate, we have to go one step further and take into account the incoherent limit as well in our theory.

Incoherent Limit

If the system is excited with a stronger field, i.e. laser pulse, the electron-photon interaction is not negligible and we have to treat it within second quantization, i.e. Eq. (2.6). Hence, the photon density n_q^μ is now our key quantity as it determines the steady-state photoluminescence by the rate of emitted photons via

$$\text{PL}(\omega_q) \propto \omega_q \frac{\partial}{\partial t} \langle c_{\mathbf{q}}^\dagger c_{\mathbf{q}} \rangle \propto \text{Im}\left[\sum_{\mathbf{k_1 k_2}\mu} M_{\mathbf{q k_1 k_2}} S_{\mathbf{k_1 k_2}}^{vc_\mu}(\omega_q)\right] \qquad (2.20)$$

The photon-assisted polarization $S_{\mathbf{k_1 k_2}}^{vc_\mu}(\omega_q)$ [44] is a measure for emitting photons with energy $\hbar\omega_q$ due to relaxation from the state $(c_\mu, \mathbf{k_2})$ in the conduction band of valley μ with the electronic momentum $\mathbf{k_2}$ to the state $(v, \mathbf{k_1})$ in the valence band with the momentum $\mathbf{k_1}$. To get access to the $S_{\mathbf{k_1 k_2}}^{vc_\mu}(\omega_q)$ we exploit Heisenberg's equation of motion again and now take into account Coulomb interaction beyond the Hartree-Fock level which gives rise to correlated quantities of the form $F_{k_1 k_2 k_3 k_4}^{\lambda_1\sigma_1\lambda_2\sigma_2\lambda_3\sigma_3\lambda_4\sigma_4} = \langle a_{k_1}^{\lambda_1\sigma_1\dagger} a_{k_2}^{\lambda_2\sigma_2} a_{k_3}^{\lambda_3\sigma_3\dagger} a_{k_4}^{\lambda_4\sigma_4} \rangle$. With this, we find

$$
\begin{aligned}
i\hbar\frac{d}{dt} S_{\mathbf{k_1 k_2 q}}^{vc_\mu} &= \left[\epsilon_{\mathbf{k_2}}^{c\uparrow} - \epsilon_{\mathbf{k_1}}^{v\uparrow} - \hbar\omega_q + \sum_{\mathbf{k}} V_{\mathbf{k_1},\mathbf{k_2},\mathbf{k}}^{ren} - i\gamma\right] S_{\mathbf{k_1 k_2 q}}^{vc_\mu} \qquad &(2.21)\\
&- \sum_{\mathbf{k}} V_{k,k_1,k_2}^{exc} S_{\mathbf{k_1-k},\mathbf{k_2-k},\mathbf{q}}^{vc_\mu} \qquad &(2.22)\\
&+ \frac{ie_0\hbar}{m}\sum_{k} g_{qk}^\mu \left(p_{k+q,k}^{cv} p_{k_1 k_2}^{vc} + F_{k+q,k,k_1,k_2}\right) \qquad &(2.23)\\
&+ \sum_{\mathbf{k}} D_{k_2 k}^{cc} S_{k_1 k q}^{vc_\mu} - D_{kk_1}^{vv} S_{kk_2 q}^{vc_\mu} \qquad &(2.24)
\end{aligned}
$$

which looks similar to the coherent limit, i.e. Eq. (2.16)-Eq. (2.19) except for the highlighted terms which account for the formation of incoherent excitons densities F_{k+q,k,k_1,k_2}.

In fact, we see that the photon-assisted polarization is driven by (i) coherent excitons $\propto |p^2|$ and (ii) incoherent exciton occupations $\propto F$.

However, since excitons play a crucial role in the optical response of TMDs we can change from the electron-hole picture to an excitonic picture, i.e. $p_{\mathbf{k_1 k_2}}^{v\uparrow c\uparrow} \rightarrow p_{\mathbf{q Q}}^\mu$ by coordinate-transformation. This will enable us to get a better understanding of excitons and direct access to the excitonic optical response both for absorption and photoluminescence.

3 Excitons in TMDs

Due to the strong Coulomb interaction in TMDs, excitons play a crucial role in the optical response of these materials [6, 14, 45]. Therefore it is convenient to change from the electron-hole picture to an excitonic picture. We will see that we can decouple the relative and center of mass motion of the excitons and find a simple expression for the excitonic optical response. Moreover, these materials show a unique band structure with direct and indirect band gaps. We will introduce here the excitonic landscape, including spin- and momentum forbidden excitons, so called "dark"; and also impurity trapped excitons, so called "localized" excitons.
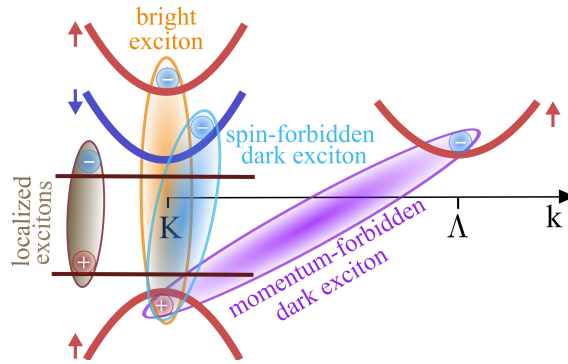

Figure 4: **The variety of excitons.** Electronic dispersion around the high symmetry K and Λ points in the Brillouin zone. Beside bright excitons (yellow), ie. both electron and hole have the same spin and momentum, there also exist dark (not optically active) excitons. Dark states can be either spin (blue) or momentum (purple) forbidden. Besides, due to local changes in the band structure, states within the band gap can appear which give rise to the formation of localized excitons (brown). Figure taken from [31].

3.1 Excitonic Basis

Our goal is to project the microscopic polarization into a new basis: $p_{\mathbf{k_1 k_2}}^{v\uparrow c\uparrow} \rightarrow p_{\mathbf{qQ}}^{v\uparrow c\uparrow}$ with center of mass $\mathbf{Q}$ and relative $\mathbf{q}$ coordinates. For this new quantities

yields:

$$\mathbf{Q} = \mathbf{k_2} - \mathbf{k_1} \quad \text{and} \quad \mathbf{q} = \alpha \mathbf{k_1} + \beta \mathbf{k_2} \tag{3.1}$$

with masses $\alpha = \frac{m_h}{m_h+m_e}$, $\beta = \frac{m_e}{m_h+m_e}$ where m_e is the electron and m_h the hole mass in the respective band. For the re-transformation we find $\mathbf{k_1} = \mathbf{q} - \beta\mathbf{Q}$ and $\mathbf{k_2} = \mathbf{q} + \alpha\mathbf{Q}$ and for the dispersion one can show that $\frac{\mathbf{k_1}^2}{2m_v} + \frac{\mathbf{k_2}^2}{2m_c} = \frac{\mathbf{q}^2}{2\mu} + \frac{\mathbf{Q}^2}{2M}$ with reduced mass $\mu = \frac{1}{m_e} + \frac{1}{m_h}$ and total mass $M = m_e + m_h$. We now project the microscopic polarization into the excitonic basis which enables us to decouple relative from center of mass movement

$$p_{\mathbf{k_1}\mathbf{k_2}}^{v\uparrow c\uparrow} \to p_{\mathbf{q}\mathbf{Q}}^{v\uparrow c\uparrow} = \sum_\mu \varphi_{\mathbf{q}}^\mu p_{\mathbf{Q}}^\mu. \tag{3.2}$$

where μ is the excitonic state, ie. bright KK and dark KΛ states or other spin- and/or momentum forbidden states. For the relative motion, we can solve the Wannier equation [5, 32]

$$\frac{\hbar^2 q^2}{2\mu}\varphi_{\mathbf{q}}^\mu - \sum_{\mathbf{k'}} V^{exc}(\mathbf{k'})\varphi_{\mathbf{q}-\mathbf{k'}}^\mu = \epsilon_\mu \varphi_{\mathbf{q}}^\mu \tag{3.3}$$

giving access to eigenenergies ϵ_μ and eigenfunctions $\varphi_{\mathbf{q}}^\mu$. With this we can now write for the excitonic dispersion:

$$E^\mu(Q) = \epsilon_\mu + \frac{\hbar^2 Q^2}{2M^\mu} \tag{3.4}$$

which enables us to put all the information of the exciton into the quantum number μ.

We find binding energies in the range of hundreds of meV and depending on the Coulomb coupling element V^{exc} the eigenenergies can be tuned.
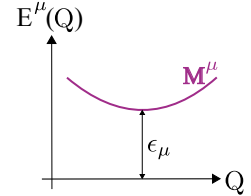
Depending on the band structure of the material, the excitonic landscape differs. We will discuss this in detail in the next section.

3.2 Exciton Landscape

Due to the complex electronic band structure of TMDs, a variety of excitons can be found which depend on the spin and momentum of the corresponding electrons and holes.
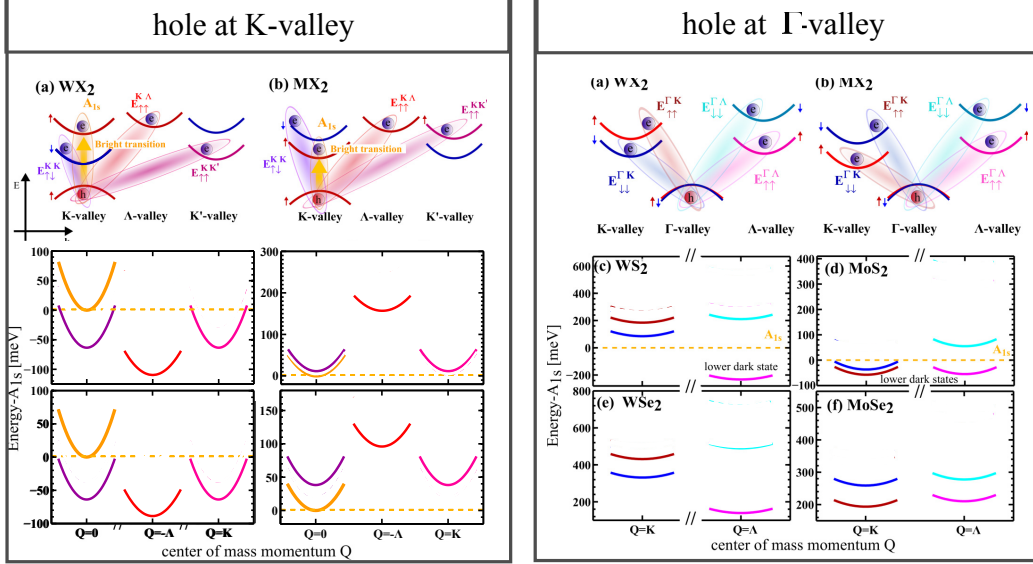
Figure 5: **Exciton landscape.** Illustration of spin or momentum forbidden excitons. Since we consider only one photon excitation processes, we assume the electron to be mobile and the hole to stay located either in the K-valley (left panel) or the Γ valley (right panel). Depending on the TMD material, the energetic order of dark and bright excitons varies. Figure taken from [22].

We mainly focus on

- BRIGHT EXCITONS: electron and hole with same spin and momentum, ie. both electron and hole are located around the K-point in the Brillouin Zone and we will call them $KK^{\uparrow\uparrow}$ excitons. This excitons are called bright because they can be directly accessed with light.

- DARK EXCITONS: electron and hole with different spin and/or momentum, ie. the electron and hole are located in different valleys and might have different spins as well. We take into account here the high symmetry points K,Λ,Γ, for example if the hole is located at the K and the electron at the Λ point with the same spin we will call it $K\Lambda^{\uparrow\uparrow}$. This excitons are called dark since they are not directly accessible by light but need a additional momentum and/or spin to become bright.

Depending on the involved valleys, each exciton has different effective mass

and hence a different binding energy and wave function, see Eq. (3.3).

PAPER I summarizes our work on the landscape of excitons and shows a detailed analysis of a variety of dark and bright excitons, see Figure 5. Especially interesting are dark states which lie energetically close to the bright state or even below. Even if they are intrinsically not accessible by light, they offer scattering channels for the decay of excitons and hence crucially influence the dynamics, in particular the lifetime, of the bright state which traces back in the linewidth in the optical spectra. A detailed analysis of scattering channels and linewidths of TMDs can be found in [24, 26, 34, 46, 47].

Interestingly, the energetic order of dark states is TMD specific. We find for: (i) excitons with the hole located at the K-valley (left panel in Figure 5) that tungsten (W) based materials exhibit both spin and momentum dark states energetically below the bright one whereas the dark states in molybdenum (M) based materials are energetically above the bright one; and (ii) excitons with the hole located at the Γ-valley (right panel in Figure 5) that only MoS_2 exhibits both momentum and spin forbidden excitons energetically below the bright one.

The different behavior stems from the electronic structure where effective masses, spin-orbit splittings and energetic distances vary between the materials due to different composition of atomic orbitals which form the bands [48, 49]. The electronic structure values are taken from density functional theory calculations (DFT) [43] as input parameters for our theory.

Dark excitons play a crucial role in the optical response of these materials since they influence *indirectly* the scattering channels and linewidth of the bright excitons [19, 20, 34, 50]. Their energetic position is still unclear and under debate in literature, and hence strategies to activate those dark states are needed to fully understand their origin. Hence a *direct* observation of the dark states in the optical spectra in form of additional peaks would be an even clearer indication of their existence and provide access to their energetic position.

On the one hand, for spin forbidden excitons, recent experiments and theory have shown their activation via magnetic fields which provides the required spin-flip [9, 19, 51].

14

On the other hand, for momentum forbidden excitons a mechanism is needed providing a momentum to the system. The focus of this work is to shed light on such mechanism. We propose that momentum forbidden excitons can be activated by molecules. Other possible mechanism include disorder or phonons [17, 26]. With this, we can calculate the excitonic spectrum by exploiting the equations of motions in excitonic basis.

3.3 Excitonic Spectrum

We can now project the equation of motions, see Eq. (2.16) -Eq. (2.19), from the electron-hole picture to the exciton picture by exploiting the separation ansatz, cf. Eq. (3.2), and projection into excitonic wave functions and get finally for the TMD Bloch equation in excitonic basis:

$$
\begin{aligned}
i\hbar \frac{d}{dt} p_{\mathbf{Q}}^{\mu} & = \left[\varepsilon_{\mu} + \frac{\hbar^2 Q^2}{2M} - i\gamma\right] p_{\mathbf{Q}}^{\mu}(t) + \Omega(t)\delta_{\mathbf{Q},\mathbf{0}} \\
& + \sum_{\nu\mathbf{k}} G_{\mathbf{Q}\mathbf{k}}^{\nu\mu} p_{\mathbf{Q}-\mathbf{k}}^{\mu}(t)
\end{aligned}
\tag{3.5}
$$

where the excitonic wave function are included in the coupling elements. Here, the Rabi frequency $\Omega(t) = \frac{ie_0\hbar}{m} \sum_{\mathbf{q}} \varphi_{\mathbf{q}}^{\mu*} \mathbf{M}_{\mathbf{q}}^{c\uparrow v\uparrow} \cdot \mathbf{A}(\mathbf{t})$ originates from the external electromagnetic field $\mathbf{A}(\mathbf{t})$ and drives polarization $p_{\mathbf{0}}^{\mu}$ which correspond to excitons with no center of mass momentum. Moreover we introduced a dephasing constant γ, including dephasing due to higher order correlations. This quantity determines the linewidth of the peaks in the excitonic spectra.

The disorder-TMD coupling in excitonic basis reads

$$
\begin{aligned}
G_{\mathbf{Q}\mathbf{k}}^{\nu\mu} & = \sum_{\mathbf{q}} \left[\varphi_{\mathbf{q}}^{\mu*} g_{\mathbf{q}-\alpha\mathbf{Q},\mathbf{q}-\alpha\mathbf{Q}+\mathbf{k}}^{cc} \varphi_{\mathbf{q}+\beta\mathbf{k}}^{\nu} - \right. \\
& \left. \varphi_{\mathbf{q}}^{\mu*} g_{\mathbf{q}+\beta\mathbf{Q}-\mathbf{k},\mathbf{q}+\beta\mathbf{Q}}^{vv} \varphi_{\mathbf{q}-\alpha\mathbf{k}}^{\nu}\right]
\end{aligned}
\tag{3.6}
$$

and drives the indirect polarization $p_{\mathbf{Q}}^{\mu}$ and hereby enables a momentum transfer.

Note that the disorder-TMD coupling can be split into intravalley processes, ie. $\nu = \mu$ which corresponds to momentum transfer within the same valley,

and also intervalley processes, ie. $\nu \neq \mu$ which corresponds to momentum transfer to other valleys. Depending on the wave function overlap of the corresponding valleys, those terms can become very strong.

Finally , by solving the TMD Bloch equation, cf. Eq. (3.5), we get access to the excitonic spectrum which exhibits a pronounced bright peak at the energy ε_{KK}. If the coupling element $G_{\mathbf{Qk}}^{\nu\mu}$ is strong enough, dark excitons will brighten up and result in an additional peak in the spectra.

The next chapter will discuss the activation via molecules in detail and shed light to what extend the optical fingerprint of the material depends on the molecular characteristics.

4 Brightening of Dark Excitons via Molecules

The high sensitivity of TMDs to their environment is the motivation to add external molecules to the layer of TMDs. The idea here is to provide the required center of mass momentum to access dark states via the molecules in a controlled way. Whereas phonons or disorder could in principle be used for the activation processes as well, molecules offer the unique possibility to be externally controlled.

In detail, we assume a non-covalent functionalization via molecules with a dipole moment, cf, Figure 6(a). Non-covalent means that the interaction between TMDs and molecules is based on weak interaction, not changing the electronic properties of the TMDs [52]. The molecules we exemplary investigate here are merocyanine/spiropyanine, exhibiting a dipole moment of 13 Debye. The choice is motivated by previous joint experiment-theory studies functionalizing carbon nanotubes and graphene with this molecules [10, 40, 53–55].
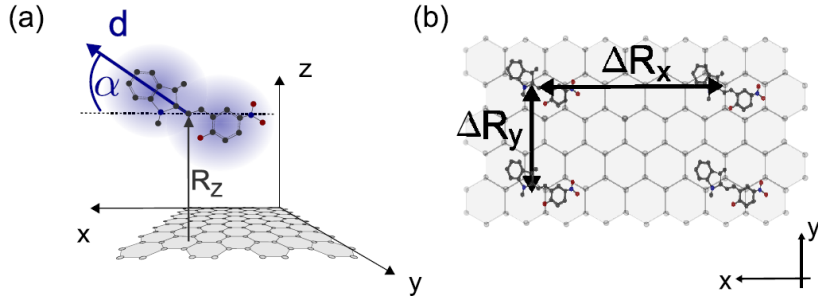
Figure 6: **Molecule configuration** (a) Randomly oriented molecule attached to the surface of the TMD in distance R_z ($\approx$ van der Waals radius). The molecules are characterized by a dipole vector $\mathbf{d}$ consisting of dipole moment d and orientation along z-axis α whereas the orientation within the xy plane is set to zero. (b) The molecules are ordered periodically with lattice constant ΔR_x and ΔR_y in x and y direction, respectively.

The molecules are characterized by a dipole vector $\mathbf{d}$ inducing interaction with excitons in the TMD material in a distance R_z. The dipole vector is

represented by dipole moment d, orientation α_d with respect to xy plane of the TMD and orientation ϕ_d in xy direction:

$$\boldsymbol{d} = d(\cos(\phi_d)\cos(\alpha_d), \sin(\phi_d)\cos(\alpha_d), \sin(\alpha_d)) \qquad (4.1)$$

Interestingly, these molecules tend to self-assemble into a periodic lattice structure under certain circumstances [56]. Motivated by this, we treat the molecules periodically with the lattice constant ΔR_x in x direction and ΔR_y in y direction, , see Figure 6(b), giving rise to a molecular density $n_{x(y)}$.

Depending on the choice of molecules, the interaction strength with the TMD varies. The next section explains under which conditions we find the strongest coupling.

4.1   Molecule-TMD Interaction

The interaction between the attached molecules and the TMD can be described in the second quantization via the carrier-molecule interaction

$$H_{c-m} = \sum_{\boldsymbol{l_1 l_2}} g_{\boldsymbol{l_1 l_2}} a_{\boldsymbol{l_1}}^\dagger a_{\boldsymbol{l_2}} \qquad (4.2)$$

with molecule-TMD coupling (MTC) element $g_{\boldsymbol{l_1 l_2}} = \langle \psi_{l_1}(\boldsymbol{r})| \sum_l \phi_l^d(\boldsymbol{r}) | \psi_{l_2}(\boldsymbol{r}) \rangle$ [54, 55].
Here, the static field induced by the molecular dipole **d** is:

$$\phi_l^d(\boldsymbol{r}) = \frac{e_0}{4\pi\epsilon_0} \frac{\boldsymbol{d} \cdot (\boldsymbol{r} - \boldsymbol{R_l})}{|\boldsymbol{r} - \boldsymbol{R_l}|^3} \qquad (4.3)$$

where $\boldsymbol{R_l}$ denotes the position of molecule l with respect to the substrate [55]. Exploiting the tight-binding approach, focusing on the energetically lowest 1s transitions and allowing only interactions with the same spin, we find for the molecule- TMD coupling (MTC) element:

$$g_{\boldsymbol{l_1 l_2}}^{\lambda_1 \lambda_2} = \frac{ie_0}{2\pi\epsilon_0} \sum_{nm} n_x n_y \delta_{|l_{1x}-l_{2x}|, \frac{2\pi n}{\Delta R_x}} \delta_{|l_{1y}-l_{2y}|, \frac{2\pi m}{\Delta R_y}} \times$$

$$\sum_j C_j^{\lambda_1 *}(\boldsymbol{l_1}) C_j^{\lambda_2}(\boldsymbol{l_2}) \delta_{\boldsymbol{l_1}-\boldsymbol{l_2}, \boldsymbol{q}} \int d\boldsymbol{q} \frac{\boldsymbol{d} \cdot \boldsymbol{q}}{|\boldsymbol{q}|^2} e^{-R_z q_z} \qquad , \qquad (4.4)$$

18

including tight-binding coefficients $C_j^{\lambda_i}$ of the corresponding high-symmetry points in the Brillouin zone (K or Λ). The most important feature here are the appearing Kronecker deltas: the periodic *molecular lattice* allows for well defined *momentum transfers* determined by the molecular lattice constant. Hence the MTC element is discrete for periodic distributions. Note that, for randomly distributed molecules, MTC allows continuous momentum transfer which will be discussed later.

We see from Eq. (4.4) that, depending on the molecular characteristics, the strength of the coupling varies. Before we discuss this in detail, we include the excitons from the TMD and define the exciton-TMD coupling as:

$$G_{\mathbf{Q}\mathbf{k}}^{\mu\nu} = \sum_{\mathbf{q}} \left[\varphi_{\mathbf{q}}^{\mu*} g_{\mathbf{q}-\alpha\mathbf{Q},\mathbf{q}-\alpha\mathbf{Q}+\mathbf{k}}^{cc} \varphi_{\mathbf{q}+\beta\mathbf{k}}^{\nu} - \varphi_{\mathbf{q}}^{\mu*} g_{\mathbf{q}+\beta\mathbf{Q}-\mathbf{k},\mathbf{q}+\beta\mathbf{Q}}^{vv} \varphi_{\mathbf{q}-\alpha\mathbf{k}}^{\nu} \right] \qquad (4.5)$$

with excitonic wave functions φ^x of the corresponding states.

Remembering the obtained the Bloch equations for the excitonic microscopic polarization $p_{\mathbf{Q}}^{\mu}$ with the index $\mu = (K, \Lambda)$ denoting the KK and $K\Lambda$ exciton:

$$\dot{p}_{\mathbf{Q}}^{KK} = \Delta\varepsilon_{\mathbf{Q}}^{K} p_{\mathbf{Q}}^{K} + \Omega\,\delta_{\mathbf{Q},\mathbf{0}} + \sum_{\mu,\mathbf{k}} G_{\mathbf{Q}\mathbf{k}}^{K\mu} p_{\mathbf{Q}-\mathbf{k}}^{K\mu}, \qquad (4.6)$$

$$\dot{p}_{\mathbf{Q}}^{K\Lambda} = \Delta\varepsilon_{\mathbf{Q}}^{\Lambda} p_{\mathbf{Q}}^{K\Lambda} + \sum_{\mu,\mathbf{k}} G_{\mathbf{Q}\mathbf{k}}^{\Lambda\mu} p_{\mathbf{Q}-\mathbf{k}}^{K\mu}, \qquad (4.7)$$

with the abbreviation $\Delta\varepsilon_{\mathbf{Q}}^{\mu} = \frac{1}{i\hbar}(\varepsilon_{\mu} + \frac{\hbar^2 Q^2}{2M_{\mu}} - i\gamma_{\mu})$, we see that the molecules enable a coupling between the two polarizations.

This coupled set of equations is illustrated in Figure 7 and can be understood as follows: the optically induced coherence $p_{\mathbf{Q}=\mathbf{0}}^{KK}$ couples to the dipoles of the adsorbed molecules and gains non-zero center of mass momentum resulting in $p_{\mathbf{Q}\neq\mathbf{0}}^{K\mu} \neq 0$. We can differentiate intervalley and intravalley coupling processes now:

1. the intravalley coupling, i.e. $\mu = K$, enable a coupling between polarizations in the same valley but with different center of mass momentum, see the yellow and red arrows in Figure 7. We find that this process is dominant for small molecular densities. As the states we can couple to
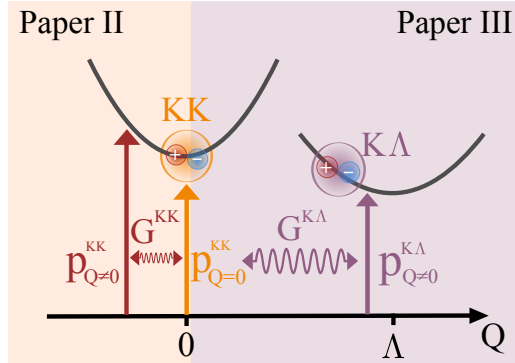
Figure 7: **Intravalley vs Intervalley coupling.** Excitonic dispersion of K and Λ valley. The external electromagnetic field drives the excitonic resonances $p_{Q=0}^K$ which can couple via the molecules either with polarizations $p_{Q\neq0}^K$ within the same valley (orange) or with polarization $p_{Q\neq0}^\Lambda$ in the Λ (purple) valley, intra and intervalley coupling respectively.

are energetically higher, we expect new optical features on the higher energy side of the bright transition.
PAPER II

2. the intervalley coupling , i.e. $\mu = \Lambda$, couples polarization in different valleys, illustrated in purple in Figure 7. This process dominates for large molecular densities. For some TMDs there exist energetically lower lying valleys which result in new peaks energetically lower then the bright exciton resonance.
PAPER III

However, when using molecules the molecular density determines the transferred center of mass momentum which gets clear by evaluating the Kronecker delta $\delta_{|\mathbf{k}|, \frac{2\pi m}{\Delta R}}$ appearing in the exciton-molecule coupling element. We see that for big distances between the molecules R, (and hence small density), small momenta are transferred whereas the tighter the molecules are packed (smaller R, larger n), the larger is the possibly transferred momentum to the system. Depending on that, either inter- or intra valley processes are dominant. Therefore we will now discuss the two processes and their dependency on external parameters.
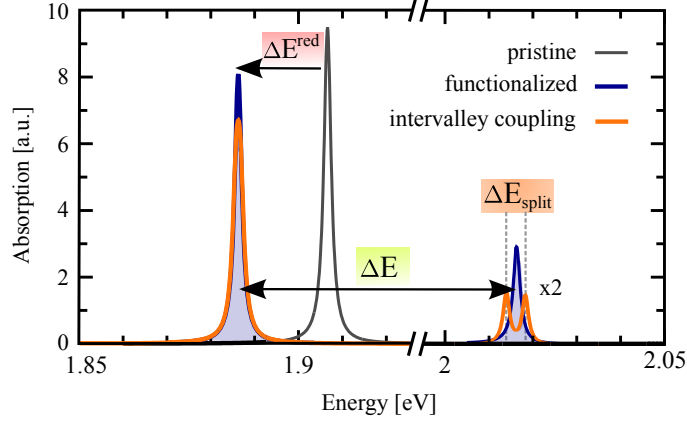
Intervalley Processes

Figure 8: **Intravalley coupling.** Excitonic absorption spectrum of pristine (black) and functionalized (blue) MoS_2. In presence of the molecules, we observe a redshift of the bright peak ΔE^{red} and an upcoming peak at the high energy side with distance ΔE from the bright resonance.

We begin with intervalley processes within the optical excited K valley. The pristine spectrum (without molecules) shows one pronounced peak at the energy of the energetically lowest transition (1.91 eV for MoS_2), see the black line in Figure 8. To reach higher states within the dispersion, only a small center of mass momentum is needed which is now provided by the molecules. In their presence, the spectra shows significant changes, see the blue line in Figure 8. First we observe an upcoming peak at higher energies corresponding to the activation of the dark states along the dispersion separated by ΔE from the bright resonance. At the same time, the bright peak shows a redshift ΔE^{red} due to back coupling from the dark to the bright state.
We can use a simple "coupled oscillator" approach to find an analytic formula for the peak position, yielding to

$$\varepsilon_{1,2} = \varepsilon_\mu + \frac{\hbar^2 Q_{xy}^2}{4M} \mp \sqrt{\left(\frac{\hbar^2 Q_{xy}^2}{4M}\right)^2 + \tilde{G}(\mathbf{Q}_{xy})} \tag{4.8}$$

Here, we have introduced the abbreviations $\tilde{G}(\mathbf{Q}_{xy}) = G_{0,\frac{2\pi}{\Delta R_x}} G_{\frac{2\pi}{\Delta R_x},\frac{2\pi}{\Delta R_x}}$.
The solutions $\varepsilon_{1,2}$ correspond to the position of the main peak (ε_1) and the

appearing side peak (ε_2) in the functionalized absorption spectra. Moreover, Eq. (4.8) reveals that the position of the resonances crucially depends on both the molecular characteristics, such as molecular coverage n, dipole moment d and dipole orientation α entering $\tilde{G}$, and on the electronic properties of the TMD entering through the total mass M.

It turns out that this formula works very well in a first approximation, for a direct comparison with the exact numerical results see Figure 9.

We want to point out that the analytic formula gives us the opportunity to understand the optical fingerprint of our system, i.e. the redshift and the peak splitting, on a fundamental level and allows us to investigate the dependence on molecular parameters.

The analytic approach enables us to the calculate the redshift of the bright resonance, i.e. $E^{red} = \epsilon_1 - \epsilon_{bright}$ for different molecule configuration. The results are summarized in Figure 9 and discussed in detail in PAPER II.

To inspire future experiments, our calculations suggest the strongest impact of the molecules for:

1. **molecular coverage in the range of 0.1 nm^{-2}** which corresponds to a distance of molecules of 3 nm. This maximum can be understood by keeping in mind that the molecules transfer a center of mass momentum and hence control which excitons will couple to each other. We find for the coupling strength $G \propto n \cdot e^{-n}$ which explains the behavior in Figure II(a) very well. On the one hand, the larger momentum difference between the excitons, the smaller the overlap of the wave functions and hence the smaller the coupling, explaining the exponential tail for higher densities. On the other hand, we find that for small densities the linear increase with n is dominant. The exact position of the maxima depends on the TMD material , which enters via the mass M in Eq. (4.8)

2. **the stronger the dipole moment the stronger is the effect**. Since we describe the interaction via a dipole interaction, this behavior is the same as for classical dipole fields which enhance the stronger the field. The exemplary mero/spiropyanine molecules are shown in Figure II(b) exemplary. However, chemists can synthesize molecules
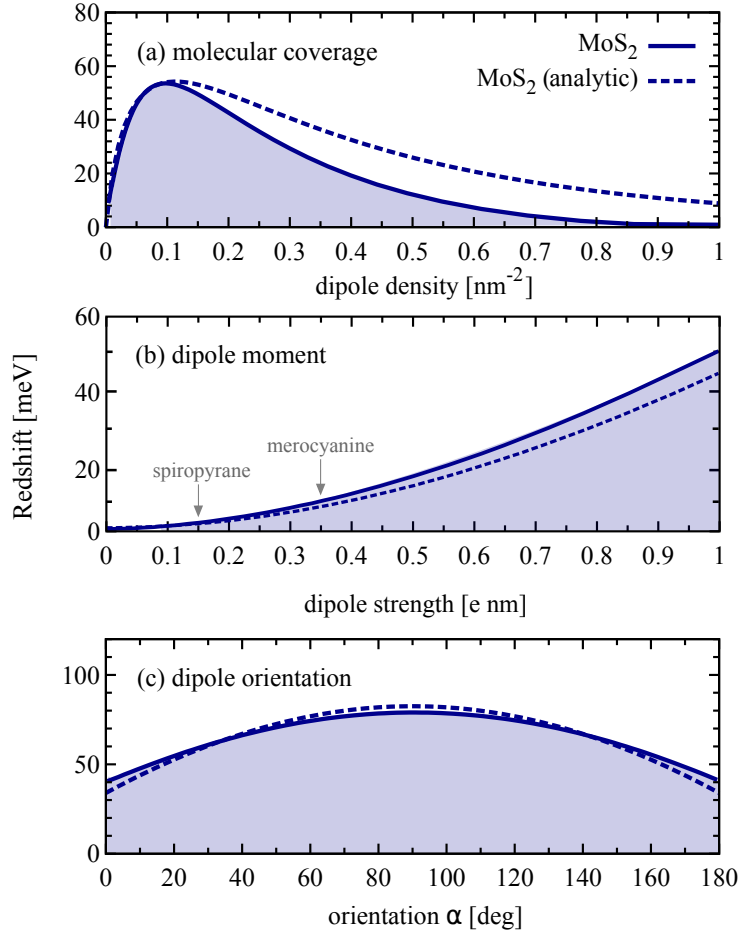
Figure 9: **Redshift dependency on dipole characteristics** Redshift of the excitonic absorption spectrum depending on functionalization parameters (a) molecular coverage, (b) dipole moment and (c) orientation. Moreover, we show the comparison between the analytic (dashed) and numeric (solid) solution which shows that the analytic solution describes the trends very well.

with even higher dipole moments in the lab which might be used for functionalizing the TMDs with the strongest impact.

3. a **perpendicular orientation** with respect to the TMD axes. This can be understood in analogy to classical dipole field where the impact is the strongest for this orientation as well.

These studies show that the spectrum can be controlled easily by the configuration of the attached molecules. The results we discussed are presented in detail in PAPER II.

So far, we have only taken into account the intravalley processes within the optically excited K valley. Interestingly, TMDs exhibit other valleys in their band structure which are energetically close to the K valley but separated by a momentum (indirect band gaps). This motivated us to include these states in our theory with the aim of activating them via the center of mass momentum provided by the molecules.

The valley of interest here is the Λ valley which is located at $Q \approx 6$ nm^{-1}. To reach this point, we assume now very densely packed molecules with intermolecular distances of 1 nm which translates into a molecular density of 1 nm^{-2}. Interestingly, the mero/spiropyran molecules packed this dense tend to self-aligned in a very ordered structure perpendicular to the surface as was shown experimentally by Tsuboi et al [56].

So naturally we have the our strong dipole moment molecules ordered in the highest-impact perpendicular directions and packed dense enough. The open question now was what happens to the overlap of the excitonic wave functions since they are located in different valleys. Hypothetically - in a perfect parabolic dispersion - being in the same valley with such a high center of mass momentum would lead to a vanishing coupling element due to vanishing overlap of wave functions and very off-resonant energetic states.

Since excitons in the Λ valley are much heavier due to lower curvatures of the band ($m_K^c = 0.36$ and $m_\Lambda^c = 0.64$ [43]) their wave functions are different and its energy is in the same range then the minimum of the K valley.

Hence the Λ valley seems very promising and indeed we find that it can be reached with the molecules efficiently. The findings are discussed in detail
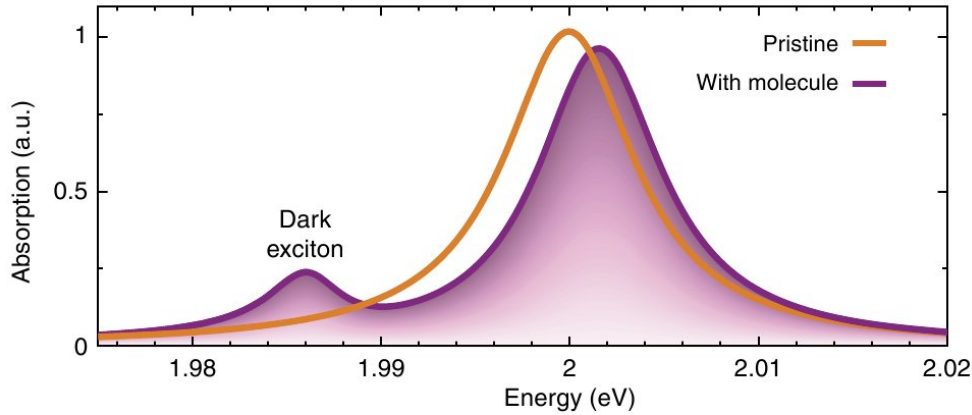
24

Figure 10: **Activation of dark exitons.** Excitonic absorption spectrum of pristine and molecule-functionalized WS_2 at 77K. Due to the efficient exciton-molecule coupling an additional peak appears energetically below the bright exciton which can be ascribed to the dark $K\Lambda$ exciton.

in PAPER III. The most important outcome is that molecules can indeed activate this dark states leading to an additional peak on the *lower energy* side of the bright exciton resonance, see Figure 10.

This *dark peak* can be used as a clear on/off trace of the attached molecules and with this the activation of dark excitons presents a new mechanism of detecting molecules.

4.2 Novel Molecule Sensing Method

Inspired by the activation of dark states via molecules, we started to study the sensitivity and dependency of the dark peak towards external parameters such as temperature and dielectric environment (determined by the substrate the TMD layer is suspended on).
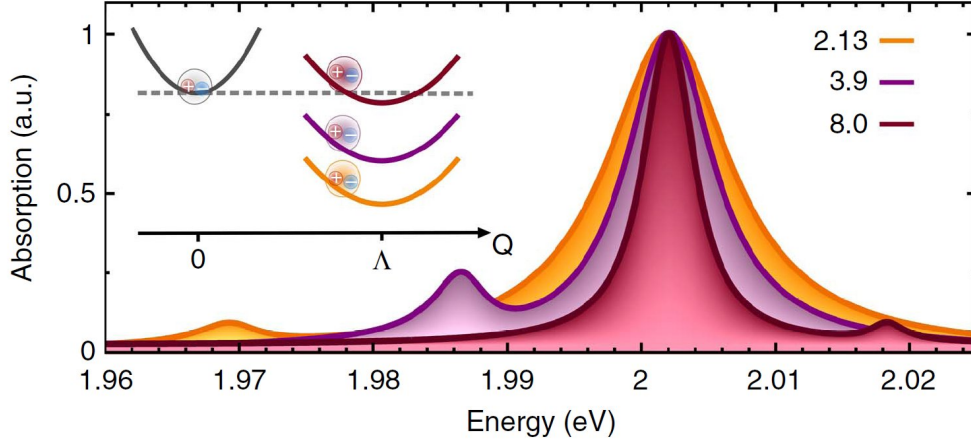
Figure 11: **Substrate dependence.** Absorption spectra for different substrates including fused silica ($\epsilon = 2.13$), silicon dioxide ($\epsilon = 3.9$) and diamond ($\epsilon = 8.0$) at 77K. For better comparison, the spectra are shifted to the main peak of silicon dioxide. The energetic position of the dark peak can be controlled by the choice of substrate since the substrate-induced screening has different impact on bright and dark excitons.

Dielectric Environment

As it is challenging to work with a freestanding monolayer of TMDs, the material is mostly suspended by a substrate. Common substrate are silicon dioxide, diamond, sapphire or hBN. The dielectric constant enters the Wannier equation, cf. Eq. (3.3), via the Keldysh potential [38]

$$V_k^{exc} = \frac{e_0^2}{\epsilon_0(\epsilon_1 + \epsilon_2)L^2} \frac{1}{|\mathbf{k}|(1 + r_0|\mathbf{k}|)}, \tag{4.9}$$

with the sample size L^2, dielectric screening constants of the surrounded media $\epsilon_{1,2}$ and screening length $r_0 = \frac{d\epsilon_\perp}{\epsilon_1 + \epsilon_2}$. The thickness d of the material is assumed to be the distance between two sulfur atoms in z direction ($d \approx 0.318$ nm [3]) and for the dielectric tensor of the TMD layer we assume only the in-plane component $\epsilon_\perp$ of the corresponding bulk material [3].

We see that the dielectric constant of the surrounding material influences the excitonic binding energy and hence the position in the spectra. Moreover, the

effect on dark and bright exciton is different due to their different excitonic masses.

This means that we can tune the position of dark and bright exciton relative to each other via the substrate, see Figure 11. Note that we normalized here to the intensity and position of the bright peak so that the we focus on the effects of the substrate on the dark peak. The purple line corresponds to our standard substrate $\epsilon = 3.9$. If the screening of the substrate is weaker (yellow line), the dark peak shifts towards lower energy and decreases in intensity whereas for higher screening (red curve) the peak shifts towards higher energies and can even shift to the energetic higher side of the bright resonance.
We also took into account changes in the broadening of the peaks due to the changed relative positions of the excitons. As the linewidth is indirect proportional to the lifetime, it is a measure how effective the scattering of excitons towards other valleys takes place. Therefore when the dark exciton is shifted towards lower energies due to weak screening, scattering from the bright to the dark states becomes more efficient, the lifetime shorter and the linewidth broader. For higher screening, the dark states shifts towards higher energies, which means that the bright state looses scattering efficiency and the line gets narrower. For details on scattering mechanisms and decay rates in TMDs see Selig et al. [24, 34]

However, our calculations show that the dark peak is visible in a broad range of possible substrates. Since high-dielectric materials tend to narrow the lines [57–59] they might be favorable for experimental setups.

Temperature Dependence

Since we investigate optical measurements of TMDs, the linewidth of the peaks is a crucial factor limiting the visibility of additional features. Therefore we studied the temperature behavior of the dark and bright exciton peak due to exciton-phonon interaction. The linewidth for the dark and bright exciton are taken from Selig et al and are calculated self-consistently [34]. The temperature behavior of the bright peak is first determined by the radiative part and then increases super-linear. For the dark peak, the linewidth is narrower as it has less scattering channels then the bright one.
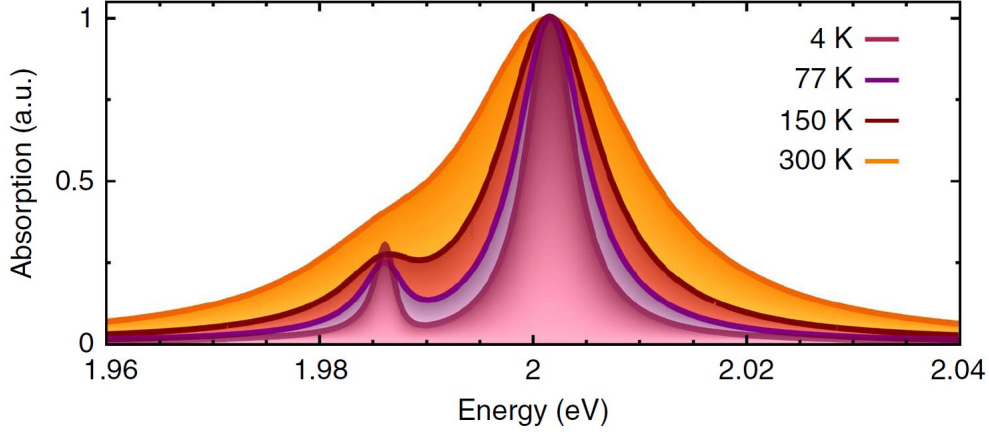
Figure 12: **Temperature dependence.** While at lower temperatures a clearly visible additional peak due to dark excitons can be observed in the absorption spectra, at room temperature only a shoulder can be seen due to increases exciton-phonon scattering and hence broader lines.

We find a pronounced dark peak up to 150 K, see orange line in Figure 12 . For room temperature (yellow curve) the dark peak is only visible as an low energy shoulder since the lines, both dark and bright, are broad. With this, we propose the best working condition for measuring the dark peak at 77 K.

Conclusion: Perfect vs Realistic Conditions

We have shown that by adding a layer of dipole molecules to the TMD surface we can activate both inter and intravalley dark states. Especially the intervalley states with the Λ valley are of fundamental interest as they could be used for a novel sensing mechanism for molecules. Our calculation reveal the best conditions for sensing for:

1. dipole moments d>10 Debye

2. dipole orientation perpendicular to the TMD surface

3. high molecular density $n \approx 1$ nm^{-2}
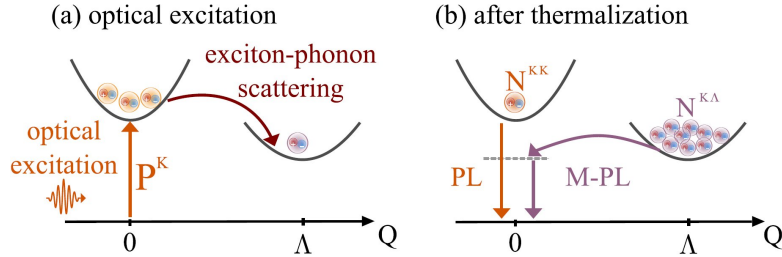
4. temperature of 150 K or below

Figure 13: **Molecule induced photoluminescence.** (a) Optical excitation induces a microscopic polarization P^K in the K valley. Due to exciton phonon interaction the polarization can decay either within K or Λ valley. Incoherent excitons N^{KK} and $N^{K\Lambda}$ are formed and thermalize until a Bose distribution is reached. (b) Whereas bright excitons N^{KK} decay radiativly by emitting a photon (PL) the dark excitons at the Λ valley require a center of mass momentum to decay back to the light cone and emit light. Molecules can provide this momentum and induce a photoluminescence signal from the dark Λ valley.

As this conditions restrict the application to a certain extend, we were looking for ideas to achieve more realistic conditions. The studies so far investigate the optical *absorption* spectra, i.e. the coherent limit. The idea is now to go one step beyond and also take into account the incoherent limit, i.e. include exciton occupation of dark and bright states to calculate *photoluminescence* spectra.

4.3   Towards Realistic Applications - Photoluminescence Spectra

Since the dark peak is energetically lower then the bright one, the idea of going to the incoherent limit and including exciton densities is that the dark state is occupied by excitons. Due to its lower position in energy we expect the dark state to be favorable for the excitons to occupy.

The efficient transfer from polarizations to populations via phonons leads to the formation of incoherent excitons on a sub-picosecond time scale [60]. The following exciton thermalization driven by emission and absorption of acoustic and optical phonons results in a thermalized exciton distribution.

Recent studies on exciton dynamics have shown that after thermalization the lower lying Λ state is indeed the one with the highest occupation [24].

This can now be exploited by the molecules which enable a molecule-induced photoluminescence (M-PL) from the dark state, see Figure 13. To implement the occupation of states in our theory, we assume Bose distributed excitons with

$$N_Q^\mu = \left[\exp\left(\frac{E_Q^\mu - \mu_{\mathrm{chem}}}{k_{\mathrm{B}}T} \right) - 1 \right]^{-1} \tag{4.10}$$

with $E_Q^\mu = \varepsilon^\mu + \frac{\hbar^2 Q^2}{2M^\mu}$, the Boltzmann constant k_{B} and the chemical potential [32] $\mu_{\mathrm{chem}} = k_{\mathrm{B}}T \ln \left[1 - \exp(-\frac{n_{\mathrm{ex}}\hbar^2 2\pi}{k_{\mathrm{B}}T 3M^\mu}) \right]$, where n_{ex} is the excitation density.

We find that the dark state is much more pronounced in photoluminescence then in absorption spectra, which was the main motivation for PAPER IV, see also Figure 14. Moreover, the intensity of the dark state can be further controlled by the excitation density, the stronger it is the stronger is the signal from the dark state. For the molecule characteristics (dipole moment/orientation/density) we find the same behavior as in absorption.

As the main goal of PAPER IV was to get closer to realistic applications, we carried out calculation on randomized molecular distributions. We find that the peaks get broader but are still clearly visible. Moreover our studies suggest that densities in range from 0.25-1 nm^{-2} could activate the dark state.

The biggest accomplishment of the photoluminescence study was, however, the much more pronounced signal of the dark peak even at higher temperatures. With this, room temperature measurement seem more realistic, as can be seen in Figure 14.

Outlook: Funtionalizing Nanomaterials

Inspired by their low-dimensionality and sensitivity to their environment we studied to what extend the optical response of TMDs changes when adding external molecules to the surface. The review article PAPER V summarizes approaches of funtionalizing carbon nanotubes, graphene and TMDs with
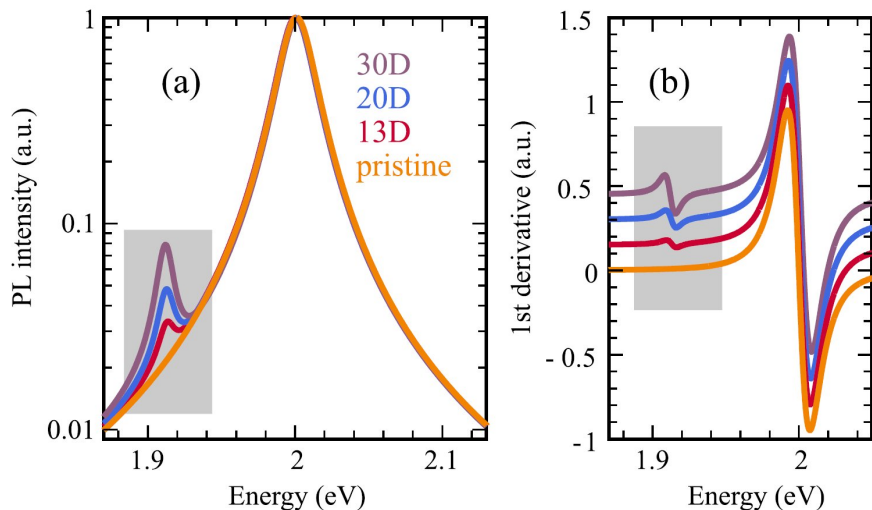
Figure 14: **Room-temperature conditions.** (a) Room-temperature PL in logarithmic plot and (b) first derivative of the PL in functionalized and pristine WS_2 for different dipole moments. The PL is normalized to the bright peak. We find that the visibility of the dark peak is in the range of 3-9 % compared to the bright peak. The main limiting factor is the broad excitonic linewidth at room temperature. Hence, we also show the derivative of the PL which shows clear traces of the dark exciton at room temperature even for 13 D. Note that the spectra are shifted along the y axes for better visibility.

dipole molecules. They all show peak shifts of the main resonances due to the coupling with molecules. However, TMDs are unique in a sense of dark excitons which offer an additional peak activated by molecules.

There are still many open questions and ideas to explore in order to bring TMDs towards sensing of environmental relevant molecules. In order to be more selective to these molecules, anchor molecules for molecules of interest could be used. Another possibility is to further investigate other molecule-TMD coupling mechanisms in combination with DFT calculations.

5 Controlling Excitons via Strain

The first part of this thesis was focused on the activation of dark states via molecules as a *direct* measurement in the optical spectra. However, even without molecules dark states leave *indirect* signatures in the optical spectra by influencing the lifetime of the bright excitons by providing additional scattering channels.

Interestingly, recent experiments have shown that TMDs are very sensitive to strain, i.e. they show significant shifts in the optical spectra and changes in the linewidth. In this part of thesis, we try to shed light on the underlying microscopic processes when straining the TMD, i.e.

1. What is the origin of the shift in the optical spectra?

2. Why is the linewidth changing differently for different TMDs?

3. Do all valleys shift in the same way?

To answer these questions, we start with an analytic approach to strain deformations in the lattice structure and identify which parts excitons play in the strained case.

5.1 Influence on Electronic and Excitonic Properties

To understand the effect of strain on the optical response, we start with the intuitively: when stretching the system, the atoms will move further away from each other. This can happen either in a uniformly way (same in x and y directions), which we will call bi-axial strain, see also middle panel in Figure 15, or the strain can be applied only in one directions, i.e. uni-axial strain corresponding to the right panel in Figure 15. Besides this pure geometric effect, i.e. a change in the lattice constant

$$a_{\text{strain}} = a_0 \cdot (1 \pm \frac{\text{strain}[\%]}{100\%}) \tag{5.1}$$

where + is for tensile and - compressive strain, the orbitals of the atoms and their overlap change. This implies changes in the hopping integrals which influence the band gap and effective mass, see Eq. (2.14).

The electronic band gap $E_{\text{gap}} = \frac{1}{2} \sum_\lambda \left(H_{ii}^\lambda - H_{jj}^\lambda \right)$ is determined by the on-site energies H_{ii}^λ. Furthermore, the nearest-neighbor hopping integral reads $H_{ij}^\lambda = t^\lambda e(\mathbf{k}) = t^\lambda \sum_\alpha e^{-i\mathbf{k}\mathbf{b}_\alpha}$ with $t^\lambda = \langle \phi_i^\lambda(\mathbf{r} - \mathbf{R_i})|H|\phi_j^\lambda(\mathbf{r} - \mathbf{R_j})\rangle$ and the nearest-neighbor connecting vectors $\mathbf{b}_\alpha$. To obtain this expression, we have exploited the symmetry of the lattice and neglected the overlap of orbital functions of neighboring sites, i.e. $S_{ij} = \langle \phi_i^\lambda|\phi_j^\lambda\rangle = \delta_{ij}$. To take changes due to strain into account, we model the orbitals with hydrogen like atomic orbitals $\phi_j(r) \propto N_j \exp^{-\frac{r-SR_j}{\sigma_j}}$ with width σ_j. Since we are not interested in the exact form of the orbitals but rather the changes due to strain, this approach is a good first attempt.

We allow the width to change with strain and find a self-consistent solution by bench-marking the theory to experimentally observed strain-induced shifts in optical spectra. Note that the reported shifts ΔE include both electronic (E_gap) and excitonic ($E_e xc^b$) effects, and our framework can now be used to differentiate those two effects. Therefore, we have self-consistently calculated both electronic and excitonic effects, and have used the reported values above as a boundary condition for the total shift.

We find that the shift in the optical spectra is mainly determined by electronic changes, see Figure 16. Taking only the electronic changes into account, we see that the pristine peak (black solid line) is shifted towards lower energies (gray dashed line). If we now include the excitonic effects as well, the peak shifts a little towards higher energies (orange curve). However, the back shift of the excitons is rather small which can be explained by the small changes in the effective masses due to strain.

PAPER VI discusses in detail the changes of excitonic binding energies and wave functions due to strain. It is worth noting that we found a softening of optical selection rules in case of uni-axial strain since the symmetry is broken when straining only in one direction.

The main message to take home from this paper is that the excitonic binding energies are rather stable under strain and change only by 5-10 meV per
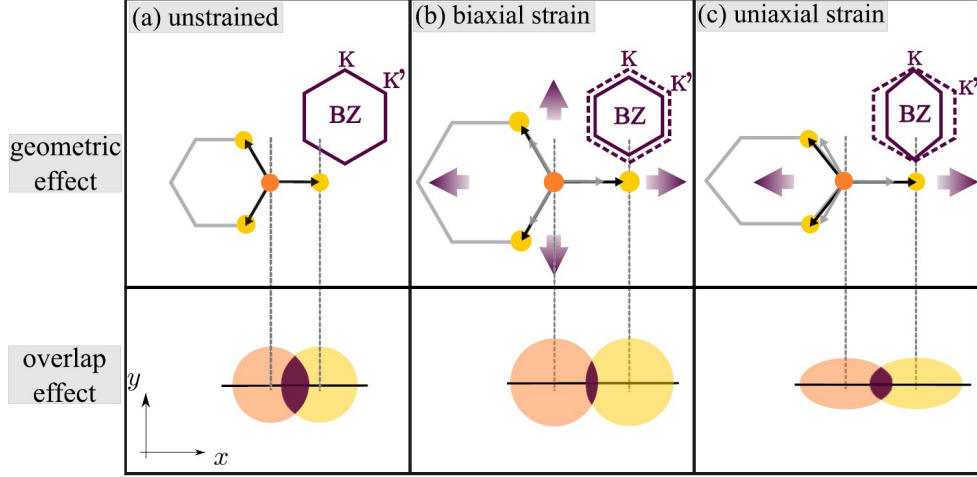
Figure 15: **Effects of strain.** Upper panel: geometric changes in real space lattice and lower panel: changes in the orbital functions. (a) The upper panel shows the hexagonal lattice in real space and the corresponding Brillouin zone in momentum space in the unstrained case. The lower represents corresponding orbital functions and their overlap. (b) In the presence of tensile bi-axial strain, atoms are uniformly moved apart. Hence, the hexagonal lattice structure remains symmetric. In momentum space, the BZ decreases. Due to larger distances between the atoms, the orbital overlap is reduced.(c) Tensile uni-axial strain, i.e. strain only along one direction (here x), and hence the hexagonal structure becomes anti-symmetric both in real and momentum space. Besides the reduced orbital overlap, the orbital functions become elliptic.

percent of strain which is, compared to the shift of 100 meV of the electronic structure, comparatively small.

So far, we only included the bright K valley for our investigations. However, having in mind the dark excitons and their importance for the lifetime, we included the effect of strain on dark excitons.
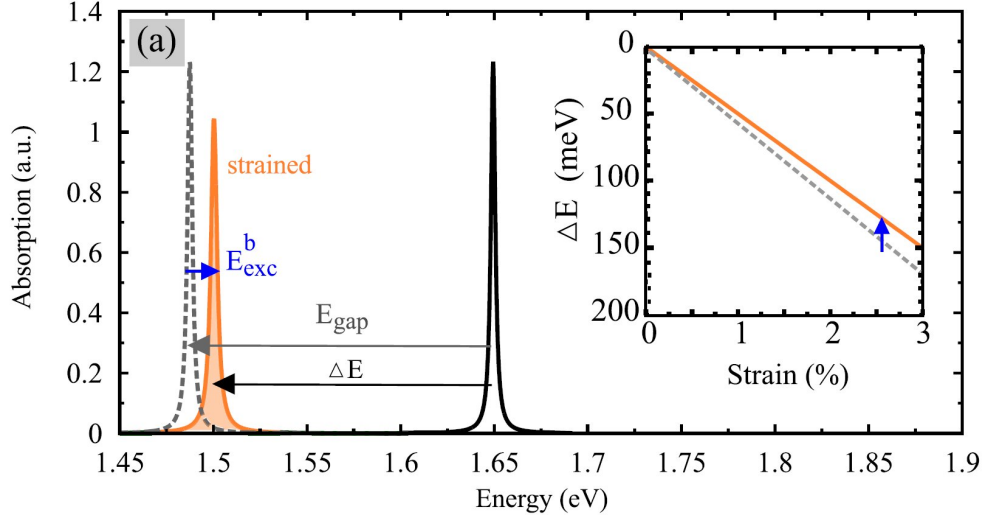
Figure 16: **Effects of strain on optical and electronic properties.** (a) Excitonic absorption spectra of unstrained (black) and uni-axially strained tungsten diselenide (WSe_2) as exemplary TMD material at 3 % strain. The observed red-shift stems from (i) a decrease in the orbital overlap giving rise to a reduced band gap (E_{gap}) and hence a red-shift (dashed gray line) and (ii) the geometric effect leading to a decrease in the effective masses, which results in weaker bound excitons (E_{exc}^b) and hence a blue-shift of the unstrained peak. The inset shows the resulting energy shift ΔE as a function of strain both with (orange) and without (gray dashed) taking into account excitonic effects.

5.2 Dark and Bright States under Strain

The ansatz we used so far to describe the electronic structure, namely assuming hydrogen-like orbitals, is too weak when including the dark states. The reason for that is that K and Λ valley are formed by different orbital functions and DFT studies have revealed different behavior for different valleys when strained [49, 57]. This is why we collaborated with DFT to include strain in the full band structure. The results are discussed in detail in Paper VII, especially with regard to linewidth changes. Surprisingly, the K and Λ valley shift in opposite directions when applying strain, see Figure 17. We find changes in the relative dark-bright separation of 150-200 meV per percent of applied strain.
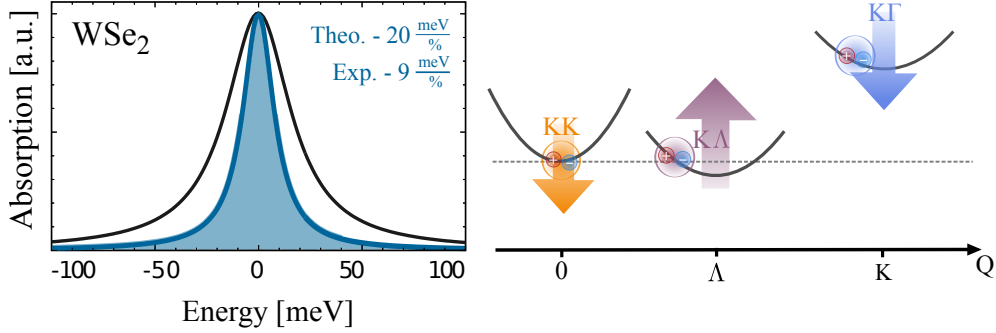
Figure 17: **Linewidth behavior with strain.** Excitonic absorption spectra with 1 % strain (blue) and without strain (black). The position of the peaks in the absorption spectrum is fixed to 0 meV. The values shown correspond to experimental and theoretical linewidth broadening. The broadening can be understood by looking at the excitonic dispersion, right panel. When tensile strain is applied, the dark Λ valley shifts up in energy and hence the bright exciton loses scattering channels, hence its lifetime gets longer and the lines narrower.

This crucially influences the linewidth of the TMD due to a change in possible scattering channels. In Figure 17 we see that in WSe_2 the linewidth decreases by -20 meV when applying 1% of tensile strain. Since the linewidth in WSe_2 is predominantly defined by scattering to the energetically lower KΛ valley, when applying tensile strain this dark states shifts up in energy and the KK excitons lose a scattering partner, resulting in longer lifetimes and narrower lines.

Our calculation are in good agreement with recent experimental data [61] which investigated the linewidth changes in different TMD materials. Depending on the relative positions of the valleys, the linewidth can increase (MoS_2), decrease (WSe_2, $MoSe_2$) or stay constant (WS_2) when applying tensile strain.

The agreement with the experiment regarding both the trends and the order of magnitude seems to underline our DFT results.
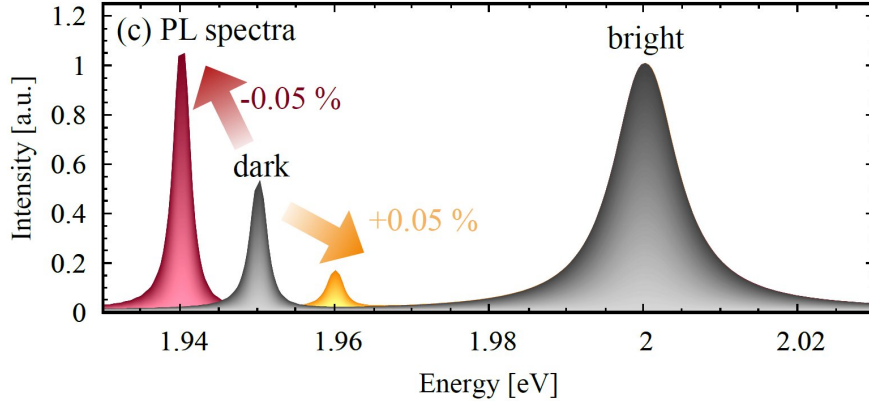
Figure 18: **Dark excitons for strain sensing.** PL spectra for WS_2 including bright resonance at 2.0 eV and activated dark resonance at 1.95 eV in the unstrained case (gray line). Applying 0.05 % tensile (compressive) strain leads to blue (red) shift and strong decrease (increase) in PL intensity of the dark peak.

5.3 Exploiting Dark Excitons for Strain Sensing

This motivated us to combine the activation of dark states (part one of this thesis) with strain. We calculated the optical response of WS_2 with an activated dark state, see gray line in Figure 18 . Note that the activation does not necessarily rely on molecules but can also be due to phonons or disorder or in general any mechanism providing a center of mass momentum to the system.

Once the dark peak is activated, it appears in the spectrum on the lower energy side. If we now apply strain to the system, we observe a shift and a change in intensity. The amount of strain implying this changes is only 0.05% which suggests TMDs a good candidates for strain sensing devices. Our calculation reveal a change of the dark-bright splitting by ±190 meV per percent of applied strain. Moreover, in the investigated range of small strain, our calculation reveal that the shifts are linear with strain.

PAPER VIII presents studies on the visibility of dark and bright peak with strain and we defined an optical gauge factor as measurement for the sensitivity of the sensor. This quantity gives the changes in the optical response,

i.e. ratio between dark and bright peak, due to the mechanical deformation. We find optical gauge factors in the range of 1000 which is huge compared to reported values for TMDs in literature so far [62, 63].

Towards Real Devices

However, there are still challenges if one is aiming towards possible real-life applications. Beside a possible usage in lab setups to measure small amounts of strain due to pressure changes, TMDs might be used as parts of health monitoring devices in form of wrist bands or similar since they are transparent and very flexible [62]. In order to use the dark exciton in this devices, the TMDs might be put to a substrate which transfers only a certain amount of mechanical strain to the TMD. In this way, the response sensitivity of the TMD could be tuned with the idea to get only a clear on/off signal from the dark peak as a response to strain.

The biggest limitation for optical devices is however given by the broadening of the lines. Since TMDs are atomically thin, they are very sensitive to impurities or disorder which naturally appear within the production process. Most kinds of disorder offer additionally scattering channels and hence lead to a broadening of the lines.

Therefore it is crucial to understand the underlying processes on a microscopic footing. Interestingly, beside the broadening effect, for certain disorder/impurity configurations there arise new, very narrow lines in the spectrum. These lines are assigned to trapped excitons by the impurity potential and are called *localized* excitons in literature and will be discussed in the next chapter.
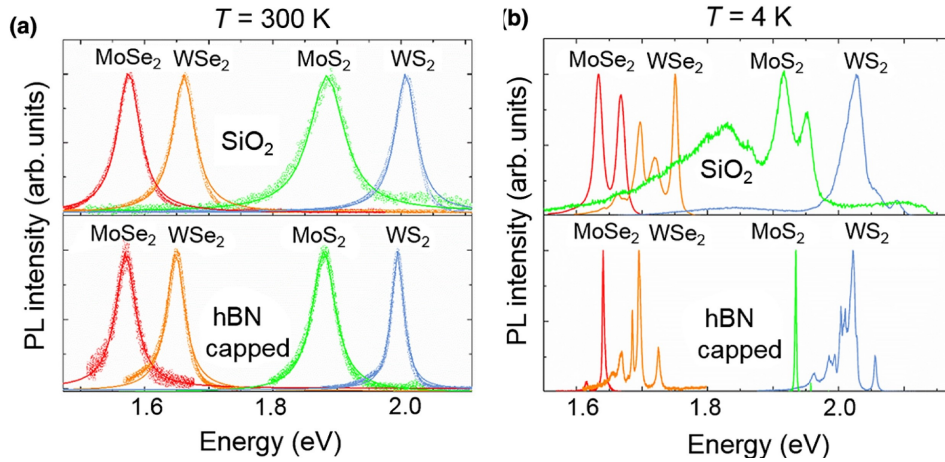
Figure 19: **Effect of encapsulation.** Photoluminescence spectra of different TMDs for (a) 300K and (b) 4K. Whereas at room temperature the encapsulation with hBN leads only to a line broadening in the spectra, at low temperatures encapsulation allows characterization of new, very narrow lines in the tungsten based materials described to as localized states. Figure taken from [64].

6 Outlook: Localizing Excitons via Impurities, Molecules and Strain

Due to their low dimensionality, nanomaterials are extremely sensitive to their environment. As we have shown in this thesis so far, this can be exploited by functionalizing them with molecules or applying strain which results both in huge changes in their optical response.

However, these materials are also sensitive to impurities due to foreign atoms or disorder stemming from the environment which reflects in uncontrolled line broadening and upcoming of "randomized" peaks in the optical spectrum. This is why a lot of effort was taken to make the samples as clean and perfect as possible. One common way of achieving this is to encapsulate the TMD layer by hBN which squeezes out all the disorder and results in very narrow lines, see Figure 19. Interestingly, at low temperatures, Figure 19(b) there seem to remain peaks with very narrow lines and high intensity in the tungsten-based materials (blue and orange lines). Their linewidth is in the
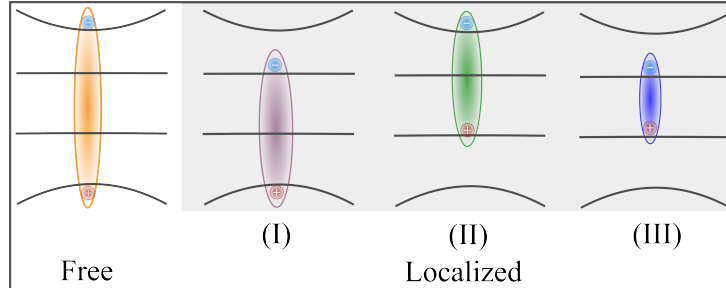
Figure 20: **Formation of localized states** Whereas free carriers show a parabolic energy dispersion, localized states are represented by mid gap states without a dispersion. The localization of carriers can appear in different ways where either (I) the electron, (II) the hole or (III) the correlated electron-hole pair is trapped by a potential.

range of μeV which means that they do have an enormously long lifetime [64]. Moreover, recent experiments reported single photon emission from these states [29, 65–68].

Our goal is to understand the origin of the localized states in order to tailor the optical properties. This could be done either by chemical or physical adsorption of defect atoms or building a nano-structured substrate inducing trapping potentials to the TMD in order to investigate the potential for novel nanoscale device applications, e.g. single-photon emitters and quantum opto-nanomechanics devices.

Presently, there are only speculations on the underlying many-particle mechanisms and the localized states appear more or less uncontrolled in the experimental setup. Hence the goal of this project is to get insights into the formation and dynamics of these localized states in order to control and tailor the optical properties.

A localized state means that the movement of the carriers is not free anymore. The localization of carriers can appear in different ways where either (I) the electron, (II) the hole or (III) the correlated electron-hole pair is trapped by a potential. In the electronic picture this can be understood as additional states within the free-particle bandgap, see Figure 20.

The appearance of the different localized states strongly depends on the

experimental setup and the induced trapping potential. Trapping can for example appear due to local strain, due to impurities in the TMDs or at the edges of the TMD sample.

Different Approaches

In order to include localized excitons in our microscopic theory, we have two different approaches:

1. Localization due to quantization of the center of mass movement

2. Localization due to an impurity potential, i.e. potential well

The first one is more empirical by starting in the excitonic picture and assuming a restriction for the center of mass momentum whereas the second approach is more fundamental by starting in the electron-hole picture and enabling a deeper understanding of the formation of these localized states.

Localization due to Quantization of the Center of Mass Movement

In general, an exciton is a correlated electron-hole pair and can be described by a center of mass momentum Q and relative momentum q. The relative momentum q can be projected in the excitonic eigenenergies and wavefunctions by solving the Wannier equation, a Schrödinger like eigenvalue problem. Hence the movement of the free electron is now fully determined by its center of mass momentum Q, eigenfunction φ^μ and its kinetic energy is simply given by a parabolic Q dependency where the curvature is given by the exciton mass

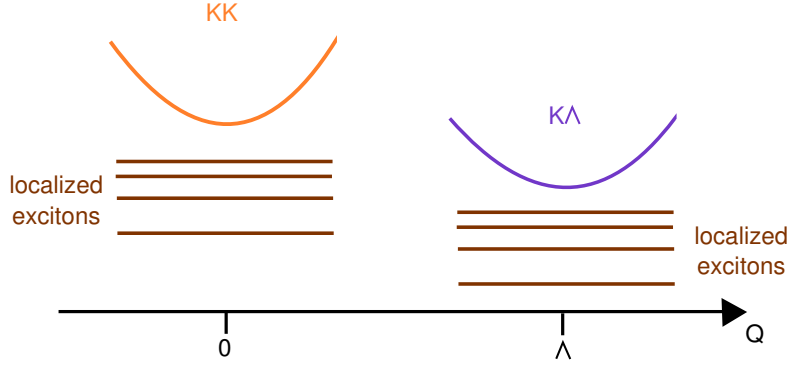$$E^\mu(Q) = \epsilon_\mu + \frac{\hbar^2 Q^2}{2M^\mu} \tag{6.1}$$

Figure 21: **Excitonic dispersion with localized states.** Illustration of excitonic dispersion, including free excitons with a parabolic dispersion as well as quantized localized excitons. Both KK and KΛ can be trapped, resulting in different energies of the corresponding localized states.

Those free excitons can now be trapped by potentials (e.g. a Gaussian potential well) which leads to a quantization of the center of mass momentum by solving again a Schrödinger like eigenvalue problem including the trapping potential
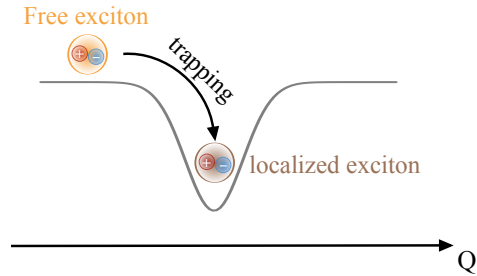
$$\left(\epsilon_\mu + \frac{\hbar^2 Q^2}{2M^\mu} - \sum_{Q'} N_\lambda e^{\frac{-\lambda^2 \cdot (Q-Q')^2}{4.0}} \right) \chi_{\mu x} = \epsilon_{\mu x} \chi_{\mu x} \qquad (6.2)$$

with new eigenvalues $\epsilon_{\mu x}$ and eigenfunctions $\chi_{\mu x}$. This results in a series of localized states which lie energetically below the free excitons. Depending on the depth and width of the trapping potential, the series of localized states changes and can be adapted to experimental measurements.

With this, one has access to both free and localized eigenenergies and wave functions and the as the next step the optical response can be calculated. Moreover, this enables calculation of exciton dynamics and relaxation, including bright, dark and localized states.

Localization due to an Impurity Potential

If we work with free carriers, the carriers can be described via plane waves and their energy is given by an effective mass approach. Due to impurities in the 2D material it can appear that a carrier is trapped (either electron or hole or both). This trapping potential can be modeled by potential wells with certain depth and width. Carriers in the trap will have energies and wave functions given by the eigenenergies/functions of the trapping potential, which can be for example a Harmonic oscillator, Poeschl-Teller, or similar. However, due to this potential, the wave function of the free carriers will change and the plane waves approach is not longer good as the carriers will feel the trapping potential. To solve this, we find a new basis, consisting of plane waves (PW) and impurity wave functions, which describe the carriers $\varphi^{\text{Loc}} = \varphi^{\text{PW}} \otimes \varphi^{\text{QD}}$.

Starting from a simple harmonic oscillator, our QD wave functions have the form:

$$\varphi_r^{\text{QD}} = \beta \sqrt{\frac{A}{\pi}} \cdot e^{\frac{-\beta^2 r^2}{2}} \tag{6.3}$$

with $\beta = \sqrt{\frac{m_{QD}^* E_{QD}}{\hbar^2}}$ with effective mass m_{QD}^* and E_{QD} energy levels of the QD which can be extracted from DFT calculations.

Within this new basis, the interaction of free-free, free-impurity and impurity-impurity carriers can now be described via Coulomb interaction, leading to free and localized excitons. The interaction between the free and localized states is here intrinsically included in the Coulomb potential. We allow electron-electron(illustrated in the sketch on the right) hole-hole, electron-hole and hole-electron scattering processes. Another possible coupling mechanism is carrier-phonon coupling.
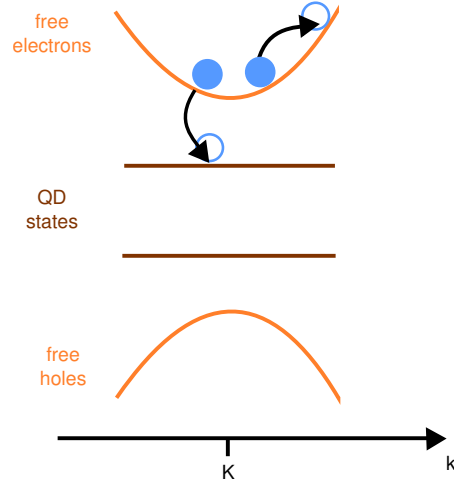
With this approach, one can find impurity dependent scattering rates which enables to calculate capture rates and dynamics. In especially, this will shed

light on the formation of localized excitons which are in this picture described by a combination of free/impurity-trapped carriers.

The goal for future projects s to combine this two approaches and to take into account different trapping potentials in order to close the gap between experiment and theory. By solving TMD Bloch equations explicitly including the coupling of optically excited free excitons with localized excitonic states, we plan to develop a theoretical framework providing microscopic understanding of photoemission channels in these nanomaterials.

7 Conclusion

In this thesis, we investigated the potential to control the optical fingerprint of transition metal dichalcogenides via external parameters, such as strain and molecules. Motivated by the TMDs perfect surface-to-volume ratio, their strong light-matter interaction and strongly bound excitons, we studied which effect molecules have on the optical response of the nanomaterial. We propose the activation of dark excitonic states due to a dipole interaction with the molecules, leading to additional peaks in the optical spectra. The position and intensity of the dark peak crucially depends on the molecular characteristics and has potential for sensor applications. In addition, we found that the dark peak is much more pronounced in the photoluminescence signal due to occupation of lower lying dark states.

Beside the direct activation of dark states, we also studied the indirect proof of their existence via the linewidth of the bright exciton resonance. Here, we focused on changes due to strain and first investigated the strain effect on excitonic binding energies and wave functions which turned out to be rather small. With help of DFT calculations we were able to calculate strain dependent shifts of dark and bright states which influence the linewidth. Moreover, we were able to explain the TMD material specific behavior very well, in good agreement with a recent experimental photoluminescence study.

We find that the dark-bright splitting is the crucial quantity for the activation and demonstration of dark states and molecule sensing. Our findindg suggest that the dark peak is much more sensitive to strain than the bright one which results in clear changes in the optical fingerprint by applying smallest amounts of strain to the system. Hence strain offers a unique possibility to tune the dark-bright splitting and offfer a possible mechanism for strain sensing.

So far, we assumed locally homogeneous strain and molecules not interacting with the electronic structure of the TMD. However, recent experiments have shown that under certain conditions spots of the TMD exhibit ultra strong photoluminescence spectra from so called localized or trapped excitons. In the second part of my PhD thesis, we want to shed light on the phenomena of localized excitons by using different trapping potentials, either induced by local strain gradients or molecules which locally induce a change in the

bandstructure and hence a potential for excitons. The goal of the future work is to reach a microscopic understanding of trapping processes and dynamics of localized excitons and explore their potential for novel technological concepts.

Acknowledgements

First, I would like to thank my supervisor, Ermin Malic, for his support, guidance and motivation during the last years. Further I would like to thank my examiner Jari Kinaret for useful comments on my thesis and Saroj Prasad Dash for being the opponent. I would also like to thank my second supervisor, Andreas Isacsson, for his support.

Moreover, I would like to thank all former and recent group members of the Malic Group. In especially, I would like to thank Samuel Brem, Malte Selig, Magdulin Dwedari and Raul Perea Causin for being my office mates and withstanding with me any small and big crisis.

A special thanks goes to my friends and family for supporting me in the good and in the bad times and always made me smile. And lastly, to my love: thank you for all the wonderful ways you make me happy.

References

[1] Andre K Geim. Nobel lecture: Random walk to graphene. *Reviews of Modern Physics*, 83(3):851, 2011.

[2] Branimir Radisavljevic, Aleksandra Radenovic, Jacopo Brivio, i V Giacometti, and A Kis. Single-layer MoS_2 transistors. *Nature Nanotechnology*, 6(3):147, 2011.

[3] Timothy C. Berkelbach, Mark S. Hybertsen, and David R. Reichman. Theory of neutral and charged excitons in monolayer transition metal dichalcogenides. *Phys. Rev. B*, 88:045318, Jul 2013.

[4] Gunnar Berghäuser and Ermin Malic. Analytical approach to excitonic properties of MoS_2. *Phys. Rev. B*, 89:125309, Mar 2014.

[5] M. Kira and S.W. Koch. Many-body correlations and excitonic effects in semiconductor spectroscopy. *Progress in Quantum Electronics*, 30(5):155 – 296, 2006.

[6] Pierluigi Cudazzo, Ilya V. Tokatly, and Angel Rubio. Dielectric screening in two-dimensional insulators: Implications for excitonic and impurity states in graphane. *Phys. Rev. B*, 84:085406, Aug 2011.

[7] Ermin Malic, Janina Maultzsch, Stephanie Reich, and Andreas Knorr. Excitonic rayleigh scattering spectra of metallic single-walled carbon nanotubes. *Phys. Rev. B*, 82(11):115439, 2010.

[8] Matthias Hirtschulz, Frank Milde, Ermin Malić, Stefan Butscher, Christian Thomsen, Stephanie Reich, and Andreas Knorr. Carbon nanotube bloch equations: A many-body approach to nonlinear and ultrafast optical properties. *Phys. Rev. B*, 77(3):035403, 2008.

[9] Andreas V Stier, Nathan P Wilson, Genevieve Clark, Xiaodong Xu, and Scott A Crooker. Probing the influence of dielectric environment on excitons in monolayer WSe_2: insight from high magnetic fields. *Nano Letters*, 16(11):7054–7060, 2016.

[10] Gunnar Berghäuser and Ermin Malic. Optical properties of functionalized graphene. *physica status solidi (b)*, 250(12):2678–2680, 2013.

[11] Damien Voiry, Anandarup Goswami, Rajesh Kappera, Cecilia de Carvalho Castro e Silva, Daniel Kaplan, Takeshi Fujita, Mingwei Chen, Tewodros Asefa, and Manish Chhowalla. Covalent functionalization of monolayered transition metal dichalcogenides by phase engineering. *Nature Chemistry*, 7(1):45–49, 2015.

[12] Yunxia Yuan, Runqing Li, and Zhihong Liu. Establishing water-soluble layered WS_2 nanosheet as a platform for biosensing. *Analytical Chemistry*, 86(7):3610–3615, 2014.

[13] Yuan Yong, Liangjun Zhou, Zhanjun Gu, Liang Yan, Gan Tian, Xiaopeng Zheng, Xiaodong Liu, Xiao Zhang, Junxin Shi, Wenshu Cong, et al. WS_2 nanosheet as a new photosensitizer carrier for combined photodynamic and photothermal therapy of cancer cells. *Nanoscale*, 6(17):10394–10403, 2014.

[14] Alexey Chernikov, Timothy C. Berkelbach, Heather M. Hill, Albert Rigosi, Yilei Li, Ozgur Burak Aslan, David R. Reichman, Mark S. Hybertsen, and Tony F. Heinz. Exciton binding energy and nonhydrogenic rydberg series in monolayer WS_2. *Phys. Rev. Lett.*, 113:076802, Aug 2014.

[15] Keliang He, Nardeep Kumar, Liang Zhao, Zefang Wang, Kin Fai Mak, Hui Zhao, and Jie Shan. Tightly bound excitons in monolayer WSe_2. *Phys. Rev. Lett.*, 113:026803, Jul 2014.

[16] Ashwin Ramasubramaniam. Large excitonic effects in monolayers of molybdenum and tungsten dichalcogenides. *Phys. Rev. B*, 86:115409, Sep 2012.

[17] Jessica Lindlau, Cedric Robert, Victor Funk, Jonathan Förste, Michael Förg, Léo Colombier, Andre Neumann, Emmanuel Courtade, Shivangi Shree, Takashi Taniguchi, et al. Identifying optical signatures of momentum-dark excitons in transition metal dichalcogenide monolayers. *arXiv preprint arXiv:1710.00988*, 2017.

[18] Jessica Lindlau, Malte Selig, Andre Neumann, Léo Colombier, Jonathan Förste, Victor Funk, Michael Förg, Jonghwan Kim, Gunnar Berghäuser, Takashi Taniguchi, et al. The role of momentum-dark excitons in the

elementary optical response of bilayer WSe$_2$. *Nature Communications*, 9(1):2586, 2018.

[19] MR Molas, Clement Faugeras, AO Slobodeniuk, Karol Nogajewski, Miroslav Bartos, DM Basko, and Marek Potemski. Brightening of dark excitons in monolayers of semiconducting transition metal dichalcogenides. *2D Materials*, 4(2):021003, 2017.

[20] You Zhou, Giovanni Scuri, Dominik S Wild, Alexander A High, Alan Dibos, Luis A Jauregui, Chi Shu, Kristiaan De Greve, Kateryna Pistunova, Andrew Y Joe, et al. Probing dark excitons in atomically thin semiconductors via near-field coupling to surface plasmon polaritons. *Nature Nanotechnology*, 12(9):856, 2017.

[21] Wei-Ting Hsu, Li-Syuan Lu, Dean Wang, Jing-Kai Huang, Ming-Yang Li, Tay-Rong Chang, Yi-Chia Chou, Zhen-Yu Juang, Horng-Tay Jeng, Lain-Jong Li, et al. Evidence of indirect gap in monolayer WSe$_2$. *Nature Communications*, 8(1):929, 2017.

[22] Ermin Malic, Malte Selig, Maja Feierabend, Samuel Brem, Dominik Christiansen, Florian Wendler, Andreas Knorr, and Gunnar Berghäuser. Dark excitons in transition metal dichalcogenides. *Phys. Rev. Mat.*, 2(1):014002, 2018.

[23] Gunnar Berghäuser, Philipp Steinleitner, Philipp Merkl, Rupert Huber, Andreas Knorr, and Ermin Malic. Mapping of the dark exciton landscape in transition metal dichalcogenides. *Phys. Rev. B*, 98(2):020301, 2018.

[24] Malte Selig, Gunnar Berghäuser, Marten Richter, Rudolf Bratschitsch, Andreas Knorr, and Ermin Malic. Dark and bright exciton formation, thermalization, and photoluminescence in monolayer transition metal dichalcogenides. *2D Materials*, 2018.

[25] Maja Feierabend, Gunnar Berghäuser, Andreas Knorr, and Ermin Malic. Proposal for dark exciton based chemical sensors. *Nature Communications*, 8:14776, 2017.

[26] Dominik Christiansen, Malte Selig, Gunnar Berghäuser, Robert Schmidt, Iris Niehues, Robert Schneider, Ashish Arora, Steffen Michaelis

de Vasconcellos, Rudolf Bratschitsch, Ermin Malic, et al. Phonon side-bands in monolayer transition metal dichalcogenides. *Phys. Rev. Lett.*, 119(18):187402, 2017.

[27] Gunnar Berghäuser, Philipp Steinleitner, Philipp Merkl, Rupert Huber, Andreas Knorr, and Ermin Malic. Mapping of the dark exciton landscape in transition metal dichalcogenides. *Phys. Rev. B*, 98(2):020301, 2018.

[28] J Jadczak, J Kutrowska-Girzycka, P Kapuściński, YS Huang, A Wójs, and L Bryja. Probing of free and localized excitons and trions in atomically thin WSe$_2$, WS$_2$, MoSe$_2$ and MoS$_2$ in photoluminescence and reflectivity experiments. *Nanotechnology*, 28(39):395702, 2017.

[29] Philipp Tonndorf, Robert Schmidt, Robert Schneider, Johannes Kern, Michele Buscema, Gary A Steele, Andres Castellanos-Gomez, Herre SJ van der Zant, Steffen Michaelis de Vasconcellos, and Rudolf Bratschitsch. Single-photon emission from localized excitons in an atomically thin semiconductor. *Optica*, 2(4):347–352, 2015.

[30] Carmen Palacios-Berraquero, Dhiren M Kara, Alejandro R-P Montblanch, Matteo Barbone, Pawel Latawiec, Duhee Yoon, Anna K Ott, Marko Loncar, Andrea C Ferrari, and Mete Atatüre. Large-scale quantum-emitter arrays in atomically thin semiconductors. *Nature Communications*, 8:15093, 2017.

[31] Thomas Mueller and Ermin Malic. 2d transition metal dichalcogenide semicondutors: exciton physics and devices. *2D Materials and Applications*, page accepted, 2018.

[32] H. Haug and S. W. Koch. *Quantum Theory of the Optical and Electronic Properties of Semiconductors.* 5th ed. (World Scientific Publishing Co. Pre. Ltd., Singapore, 2004).

[33] A. Knorr, S. Hughes, T. Stroucken, and S.W. Koch. Theory of ultrafast spatio-temporal dynamics in semiconductor heterostructures. *Chemical Physics*, 210(12):27 – 47, 1996. Confined Excitations in Molecular and Semiconductor Nanostructures.

[34] Malte Selig, Gunnar Berghäuser, Archana Raja, Philipp Nagler, Christian Schüller, Tony F Heinz, Tobias Korn, Alexey Chernikov, Ermin

Malic, and Andreas Knorr. Excitonic linewidth and coherence lifetime in monolayer transition metal dichalcogenides. *Nature Communications*, 7:13279, 2016.

[35] Ermin Malic and Andreas Knorr. *Graphene and Carbon Nanotubes: Ultrafast Optics and Relaxation Dynamics*. John Wiley & Sons, 2013.

[36] Di Xiao, Gui-Bin Liu, Wanxiang Feng, Xiaodong Xu, and Wang Yao. Coupled spin and valley physics in monolayers of MoS_2 and other group-vi dichalcogenides. *Phys. Rev. Lett.*, 108:196802, May 2012.

[37] H. Ochoa and R. Roldán. Spin-orbit-mediated spin relaxation in monolayer MoS_2. *Phys. Rev. B*, 87:245421, Jun 2013.

[38] Keldysh. *JETP Lett.*, 29:658, 1978.

[39] Gunnar Berghäuser, Andreas Knorr, and Ermin Malic. Optical fingerprint of dark 2p-states in transition metal dichalcogenides. *2D Materials*, 4(1):015029, 2016.

[40] E Malic, A Setaro, P Bluemmel, Carlos F Sanz-Navarro, Pablo Ordejn, S Reich, and A Knorr. Carbon nanotubes as substrates for molecular spiropyran-based switches. *Journal of Physics: Condensed Matter*, 24(39):394006, 2012.

[41] Dong Hoon Keum, Suyeon Cho, Jung Ho Kim, Duk-Hyun Choe, Ha-Jun Sung, Min Kan, Haeyong Kang, Jae-Yeol Hwang, Sung Wng Kim, Heejun Yang, et al. Bandgap opening in few-layered monoclinic mote 2. *Nature Physics*, 11(6):482, 2015.

[42] Graeme Cunningham, Damien Hanlon, Niall McEvoy, Georg S Duesberg, and Jonathan N Coleman. Large variations in both dark-and photoconductivity in nanosheet networks as nanomaterial is varied from MoS_2 to WTe_2. *Nanoscale*, 7(1):198–208, 2015.

[43] Andor Kormanyos, Guido Burkard, Martin Gmitra, Jaroslav Fabian, Viktor Zolyomi, Neil D Drummond, and Vladimir Falko. k p theory for two-dimensional transition metal dichalcogenide semiconductors. *2D Materials*, 2(2):022001, 2015.

[44] A Thränhardt, S Kuckenburg, A Knorr, T Meier, and SW Koch. Quantum theory of phonon-assisted exciton formation and luminescence in semiconductor quantum wells. *Phys. Rev. B*, 62(4):2706, 2000.

[45] A Steinhoff, M Rosner, F Jahnke, TO Wehling, and C Gies. Influence of excited carriers on the optical and electronic properties of MoS_2. *Nano Letters*, 14(7):3743–3748, 2014.

[46] Gunnar Berghäuser, Ivan Bernal-Villamil, Robert Schmidt, Robert Schneider, Iris Niehues, Paul Erhart, Steffen Michaelis de Vasconcellos, Rudolf Bratschitsch, Andreas Knorr, and Ermin Malic. Inverted valley polarization in optically excited transition metal dichalcogenides. *Nature Communications*, 9(1):971, 2018.

[47] Ivan Bernal-Villamil, Gunnar Berghäuser, Malte Selig, Iris Niehues, Robert Schmidt, Robert Schneider, Philipp Tonndorf, Paul Erhart, Steffen Michaelis de Vasconcellos, Rudolf Bratschitsch, et al. Exciton broadening and band renormalization due to dexter-like intervalley coupling. *2D Materials*, 5(2):025011, 2018.

[48] Chung-Huai Chang, Xiaofeng Fan, Shi-Hsin Lin, and Jer-Lai Kuo. Orbital analysis of electronic structure and phonon dispersion in MoS_2 , $MoSe_2$, WS_2 , and WSe_2 monolayers under strain. *Phys. Rev. B*, 88(19):195420, 2013.

[49] Qu Yue, Jun Kang, Zhengzheng Shao, Xueao Zhang, Shengli Chang, Guang Wang, Shiqiao Qin, and Jingbo Li. Mechanical and electronic properties of monolayer MoS_2 under elastic strain. *Phys. Lett. A*, 376(12):1166–1170, 2012.

[50] Akshay Singh, Andreas Knorr, Chandriker Kavir Dass, Chang-Hsiao Chen, Ermin Malic, Galan Moody, Genevieve Clark, Gunnar Berghäuser, Kai Hao, Kha Tran, et al. Intrinsic homogeneous linewidth and broadening mechanisms of excitons in monolayer transition metal dichalcogenides. *Nature Communications*, 6:8315, 2015.

[51] M Koperski, MR Molas, A Arora, K Nogajewski, M Bartos, J Wyzula, D Vaclavkova, P Kossacki, and M Potemski. Orbital, spin and valley contributions to zeeman splitting of excitonic resonances in MoSe2, WSe 2 and WS 2 monolayers. *arXiv preprint arXiv:1803.00376*, 2018.

[52] Andreas Hirsch and Otto Vostrowsky. *Functional Molecular Nanostructures.* Springer Berlin Heidelberg, Berlin, Heidelberg, 2005.

[53] E. Malic, C. Weber, M. Richter, V. Atalla, T. Klamroth, P. Saalfrank, S. Reich, and A. Knorr. Microscopic model of the optical absorption of carbon nanotubes functionalized with molecular spiropyran photoswitches. *Phys. Rev. Lett.*, 106(9):097401, March 2011.

[54] Gunnar Berghäuser and Ermin Malic. Moleculesubstrate interaction in functionalized graphene. *Carbon*, 69:536 – 542, 2014.

[55] E. Malic, C. Weber, M. Richter, V. Atalla, T. Klamroth, P. Saalfrank, S. Reich, and A. Knorr. Microscopic model of the optical absorption of carbon nanotubes functionalized with molecular spiropyran photoswitches. *Phys. Rev. Lett.*, 106:097401, Mar 2011.

[56] Kazuma Tsuboi, Kazuhiko Seki, Yukio Ouchi, Katsuhiko Fujita, and Kotaro Kajikawa. Formation of merocyanine self-assembled monolayer and its nonlinear optical properties probed by second-harmonic generation and surface plasmon resonance. *Japanese Journal of Applied Physics*, 42(2R):607, 2003.

[57] Qing Hua Wang, Kourosh Kalantar-Zadeh, Andras Kis, Jonathan N Coleman, and Michael S Strano. Electronics and optoelectronics of two-dimensional transition metal dichalcogenides. *Nature Nanotechnology*, 7(11):699, 2012.

[58] Lutz Waldecker, Archana Raja, Roland Koch, Aaron Bostwick, Chris Jozwiak, Eli Rotenberg, and Tony Heinz. Bandgap renormalization and band offset in 2d materials caused by dielectric screening. *Bulletin of the American Physical Society*, 2018.

[59] Aïda Hichri, Imen Ben Amara, Sabrine Ayari, and Sihem Jaziri. Exciton center-of-mass localization and dielectric environment effect in monolayer WS_2. *Journal of Applied Physics*, 121(23):235702, 2017.

[60] Samuel Brem, Malte Selig, Gunnar Berghaeuser, and Ermin Malic. Exciton relaxation cascade in two-dimensional transition metal dichalcogenides. *Scientific Reports*, 8(1):8238, 2018.

[61] Iris Niehues, Robert Schmidt, Matthias Drüppel, Philipp Marauhn, Dominik Christiansen, Malte Selig, Gunnar Berghäuser, Daniel Wigger, Robert Schneider, Lisa Braasch, et al. Strain control of exciton–phonon coupling in atomically thin semiconductors. *Nano Letters*, 18(3):1751–1757, 2018.

[62] Minhoon Park, Yong Ju Park, Xiang Chen, Yon-Kyu Park, Min-Seok Kim, and Jong-Hyun Ahn. MoS_2-based tactile sensor for electronic skin applications. *Advanced Materials*, 28(13):2556–2562, 2016.

[63] Meng-Yen Tsai, Alexey Tarasov, Zohreh R Hesabi, Hossein Taghinejad, Philip M Campbell, Corey A Joiner, Ali Adibi, and Eric M Vogel. Flexible MoS_2 field-effect transistors for gate-tunable piezoresistive strain sensors. *ACS Applied Materials & Interfaces*, 7(23):12850–12855, 2015.

[64] F Cadiz, E Courtade, C Robert, G Wang, Y Shen, H Cai, T Taniguchi, K Watanabe, H Carrere, D Lagarde, et al. Excitonic linewidth approaching the homogeneous limit in MoS_2-based van der waals heterostructures. *Phys. Rev. X*, 7(2):021026, 2017.

[65] Chitraleema Chakraborty, Laura Kinnischtzke, Kenneth M Goodfellow, Ryan Beams, and A Nick Vamivakas. Voltage-controlled quantum light from an atomically thin semiconductor. *Nature Nanotechnology*, 10(6):507, 2015.

[66] M Koperski, K Nogajewski, A Arora, V Cherkez, P Mallet, J-Y Veuillen, J Marcus, P Kossacki, and M Potemski. Single photon emitters in exfoliated WSe_2 structures. *Nature Nanotechnology*, 10(6):503, 2015.

[67] Yu-Ming He, Genevieve Clark, John R Schaibley, Yu He, Ming-Cheng Chen, Yu-Jia Wei, Xing Ding, Qiang Zhang, Wang Yao, Xiaodong Xu, et al. Single quantum emitters in monolayer semiconductors. *Nature Nanotechnology*, 10(6):497, 2015.

[68] Ajit Srivastava, Meinrad Sidler, Adrien V Allain, Dominik S Lembke, Andras Kis, and A Imamoğlu. Optically active quantum dots in monolayer WSe_2. *Nature Nanotechnology*, 10(6):491, 2015.